INVESTIGATION OF POLY(LACTIC ACID)/POLYOXY METHYLENE BLENDS: CRYSTALLIZATION BEHAVIOR AND HEAT RESISTANCE

By

XIAOJIE GUO

A thesis submitted in partial fulfillment of
the requirements for the degree of

Master of Science in Materials Science and Engineering

WASHINGTON STATE UNIVERSITY
School of Mechanical and Materials Engineering

August 2012

To the Faculty of Washington State University:

The members of the Committee appointed to examine the thesis of XIAOJIE GUO find it satisfactory and recommend that it be accepted.

Jinwen Zhang, Ph.D., Chair

Michael P. Wolcott, Ph.D.

Vikram Yadama, Ph.D.

ACKNOWLEDGEMENT

I would like to give my special thanks to committee chair and my advisor, Dr. Jinwen Zhang, for his constant professional guidance and patience in supervision. Meanwhile, I am appreciated for the assistance and dedication from committee member, Drs. Michael P. Wolcott and Vikram Yadama. I would like to express my gratitude to Dr. Hongzhi Liu, who constantly provided constructive advice and instructions through my whole experiments. I also feel grateful to the faculty and staff of the Composite Materials and Engineering Center such as Bob Duncan, Suzanne Hamada, Janet Duncan and Scott Lewis: without their assistance and support during the last four years, I won’t able to complete my thesis. Finally, a special sign of appreciation goes to my parents and husband for their unconditional support to me while completing my graduate degree.

INVESTIGATION OF POLY(LACTIC ACID)/POLYOXY METHYLENE BLENDS: CRYSTALLIZATION BEHAVIOR AND HEAT RESISTANCE

ABSTRACT

By Xiaojie Guo, M.S.

Washington State University

August 2012

Chair. Jinwen Zhang

In this research, poly(lactic acid) (PLA)/polyoxymethylene (POM) was prepared through melt extrusion. Crystallizations of neat PLA and PLA in the presence of POM were investigated by differential scanning calorimetry (DSC), polarized optical microscope and X-ray diffraction (XRD) in detail for a comparative study of the effects of different fillers on the crystallization and morphology of PLA. The results suggest that the crystal structure of PLA remained unchanged by the addition of POM, while the crystallization ability of PLA was enhanced in the presence of POM. The PLA/POM blends presented higher light transmittance than neat PLA and the PLA/talc blends, indicating POM was partially miscible with PLA, which was

consistent with the FTIR results. Well-defined banded spherulites were found in the case of PLA/POM blends during isothermal crystallization. The thermodynamic properties and phase morphology were examined using dynamic mechanical analysis (DMA), differential scanning calorimetry (DSC) and scanning electron microscopy (SEM). Heat deflection temperature (HDT) of PLA was improved by incorporating POM, a highly crystalline polymer with excellent heat resistance. The HDT of neat PLA was increased nearly 2-fold from 65.5 ^{o}C to 133 ^{o}C by adding 50 wt% POM. Multiple-crack structure was observed on the surface of the PLA blends containing high POM content. Fox equation was used to assess the miscibility of the PLA/POM blends and showed that the PLA/POM blends were partially miscible, which was consistent with the FTIR results in which a distinctive characteristic peak around at 1000 cm^{-1} for PLA/POM blends indicated partially miscible. The toughening effects of two elastomers on the PLA/POM blend (50/50), i.e. thermoplastic polyurethane (TPU) and poly(ethylene-glycidyl methacrylate) (EGMA), were investigated in detail in this study. The experimental results suggested that TPU was more effectively on toughening the PLA/POM blend than EGMA.

TABLE OF CONTENTS

page

ACKNOWLEDGEMENT iii

ABSTRACT iv

LIST OF TABLES viii

LIST OF FIGURES ix

Chapter 1 Introduction 1

1.1 Why biobased plastics 1

1.2 Development, synthesis and application of PLA 2

1.3 Effects of various nucleating agents on PLA crystallization 4

1.4 Methods and development of enhancing heat resistance of PLA 8

1.5 Research objectives 9

References 12

Chapter 2 Crystallization and morphology of PLA Blends 15

Abstract 15

2.1 Introduction 16

2.2 Experimental 18

2.3 Results and discussion 22

2.4 Conclusions 61

Reference 63

Chapter 3 Properties and structure of PLA/POM blends with excellent heat resistance 66

Abstract 66

3.1 Introduction 67

3.2 Experimental 69

3.3 Results and discussion 73

Chapter 4 Conclusions 93

LIST OF TABLES

Page

Table 1.1. HDT values of various PLA blends published by NatureWorks LLC. 9

Table 2.1. Characteristics of materials used in this study 18

Table 2.2. DSC parameters of melting and crystallization for neat PLA, POM and the PLA/POM blends 25

Table 2.3. DSC parameters of cooling and crystallization for neat PLA, POM and the PLA/POM blends 26

Table 2.4. Isothermal crystallization kinetics parameters for neat PLA and its two blends of POM and talc on the Avrami equation 36

Table 2.5. Mechanical Properties of neat PLA and its two blends with POM and talc61

Table 3.1. Characteristics of materials in this study 69

Table 3.2. Glass transition temperature of the PLA/POM blends and its components (neat PLA and POM) 76

Table 3.3. DSC parameters of cooling and crystallinity for the PLA/POM blends..... 77

Table 3.4. HDT of PLA, POM and their blends 80

Table 3.5. HDT of the PLA/POM blends with and without heat treatment..... 82

Table 3.6. Mechanical Properties of neat PLA, neat POM and their blends 86

Table.7. Mechanical properties of neat PLA, POM50 and its two ternary blends..... 87

LIST OF FIGURES

page

Figure 1.1. Synthesis of poly(lactic acid) 3

Figure 2.1. First heating DSC curves of neat PLA, POM and the PLA/POM blends 24

Figure 2.2 First heating DSC curves of neat PLA, POM and the PLA/POM blends 24

Figure 2.3. First cooling DSC curves of neat PLA, POM and the PLA/POM blends 25

Figure 2.4. First cooling curves of neat PLA and PLA/POM blends 26

Figure 2.5. Second heating of neat PLA, POM and the PLA/POM blends 28

Figure 2.6. Crystallization isotherms of neat PLA, PLA/POM blends and PLA/talc blends at 108 ^{o}C. The curves were vertically shifted for legibility 29

Figure 2.7. Curves of heat flow versus time for the isothermal crystallization of neat PLA, PLA/POM blends and PLA/talc blends 32

Figure 2.8. Curves of relative crystallinity versus time for isothermal crystallization of neat PLA, PLA/POM blends and PLA/talc blends 34

Figure 2.9. Curves of log{-ln[1-X(t)]} versus log t for isothermal crystallization of neat PLA, PLA/POM blends and PLA/talc blends..... 36

Figure 2.10. Curve of the half-time of crystallization versus different weight fractions of POM and talc respectively in the PLA/POM blends 39

Figure 2.11. Curve of the half-time of crystallization versus different

crystallization temperatures of neat PLA and its two blends with POM and talc. 40

Figure 2.12. Curves of heat flow versus temperature for nonisothermal crystallization of PLA/POM=95/5 at different cooling rates 42

Figure 2.13. Curves of relative crystallization versus (a) crystallization temperature and (b) time for nonisothermal crystallization of PLA/POM=95/5.. 43

Figure 2.14. Dependency of the melt-crystallization peak temperature on the cooling rate (R) for nonisothermal crystallization of PLA/POM=95/5 44

Figure 2.15. Polarized optical micrographs of neat PLA, neat POM, PLA/POM blends and PLA/talc blends isothermally crystallized at 130 ^{o}C 46

Figure 2.16. Crystalline growth of neat PLA during isothermal crystallization at 130 ^{o}C, the corresponding crystallization time is given in the graphs 48

Figure 2.17. Crystalline growth of PLA/POM blends (PLA/POM=95/5) during isothermal crystallization at 130 ^{o}C, the corresponding crystallization time is given in the graphs 49

Figure 2.18. Polarized optical micrographs of the PLA/POM blends with vatious POM content:(a) 5; (b) 10; (c) 20; (d) 25; (e) 35; (f) 50 wt% 51

Figure 2.19. Photographs of neat PLA and PLA blends with POM and talc on a background paper for demonstrating their transparency 52

Figure 2.20. UV-vis transmittance spectra of neat PLA, neat POM, PLA/POM blends and PLA/talc blends 53

Figure 2.21. XRD patterns of neat POM, neat PLA and the PLA/POM blends, all film samples were isothermally hold at 120 oC for 45 min..... 55

Figure 2.22. XRD patterns of neat PLA and its two blends with POM and talc, all films samples were quenched from the melt 57

Figure 2.23. FTIR spectra in the wavenumber range of 700-1600 cm-1 of neat POM, neat PLA and PLA/POM blends 57

Figure 2.24. Deconvolution curve of neat POM in the wavenumber range 900-1050 cm^{-1} 58

Figure 2.25. Cryo-fractured SEM images of blends: (a) neat PLA, (b) POM1, (c) POM2 and (d) POM5 60

Figure 3.1. Dynamic mechanical properties of the PLA/POM blends: (a) strorage modulus, (b) loss modulus and (c) tan δ 74

Figure 3.2. First cooling DSC curves of the PLA/POM blends 77

Figure 3.3. Dynamic mechanical properties of the PLA/POM lends 79

Figure 3.4. HDT of the PLA/POM blends 79

Figure 3.5. Dynamic mechanical properties of the PLA/POM blends with and without heat treatment 81

Figure 3.6. FTIR spectra in the wavenumber range of 700-1600 cm^{-1} of neat POM, neat PLA and PLA/POM blends 83

Figure 3.7. Cryo-fractured SEM images of the PLA/POM blends: (a) neat PLA, (b) neat POM, (c) POM5, (d) POM10, (e) POM25 and (f) POM50 85

Figure 3.8. Impact strength of ternary blends versus elastomer content 88

Chapter 1 Introduction

1.1 Why biobased plastics

Conventional synthetic petroleum-based polymers such as polyethylene (PE), polypropylene (PP), polystyrene (PS), poly(ethylene terephthalate) (PET), and polyvinyl chloride (PVC) used to shared a major share of commodity plastics (Amass et al., 1998). The non-degradability, non-renewability, emissions of greenhouse gases and the diminishment of petroleum resources during production and incineration of conventional synthetic petroleum-based polymers have restricted the versatility and applications of these polymers. Concerns over the environmental issues and sustainability of conventional petroleum-based synthetic polymer materials have motivated a paradigm shift in developing biobased polymers, blends and composites from renewable resources as potential substitutes to replace the conventional petroleum-based polymers for the commodity applications. Abundant renewable resources such as agricultural feedstocks used for the production of biomaterials can facilitate the transition from nonrenewable sources to renewable bioresources (Ragauskas et al., 2006). The global market for bioplastics was 291 thousand tons in year 2007 and is estimated to touch 2.1 million tons by year 2017 (Bioplastics - Global Market Overview, New York, Jan. 4, 2012;). The bio-based polymers such as poly(lactic acid) (PLA), polyhydroxyalkanoates (PHAs) and biobased poly(trimethylene terephthalate) (PTT) are examples of biologically derived materials

developed for mainstream applications (Carole et al., 2004; Kurian et al., 2005).

1.2 Development, synthesis and application of PLA

Among a few commercially biobased polymer plastics, PLA is the most promising sustainable alternative to petroleum-based plastics and has been investigated more than the rest. The primary interest in these biobased polymers is due to the production of their precursor, lactic acid from renewable resources such as sugarcane, sugar beet and corn starch (Drumright et al., 2000). The method of polymerizing lactic acid was first introduced by Carothers in 1932 (Holten et al 1971), but the breakthrough in pilot production of PLA was achieved by Cargill in 1992. Currently NatureWorks with the PLA production capacity of 280 thousand tons annually, is the single largest producer of PLA. PLA has been used in biomedical applications such as tissue implants and surgical suture since several decades ago while its use as a commercial commodity thermoplastic was obtained only in the last two decades. Wal-Mart, the world's largest retailer started using PLA in packaging applications in the beginning of November 2005. The current applications of PLA are in packaging, textile, and electronics (Bhardwaj et al 2007).

PLA is synthesized either through polycondensation of lactic acid (2-hydroxy propionic acid) or ring-opening polymerization of lactide (the dimer of lactic acids), as illustrated in Figure 1.1. The monomer, lactic acid, can be produced via bacterial fermentation using enzyme thinned cornstarch or sugar directly as carbon sources. Lactic acid is one of the simplest chiral molecules and exists as the two stereo isomers:

L- and D-lactic acid.

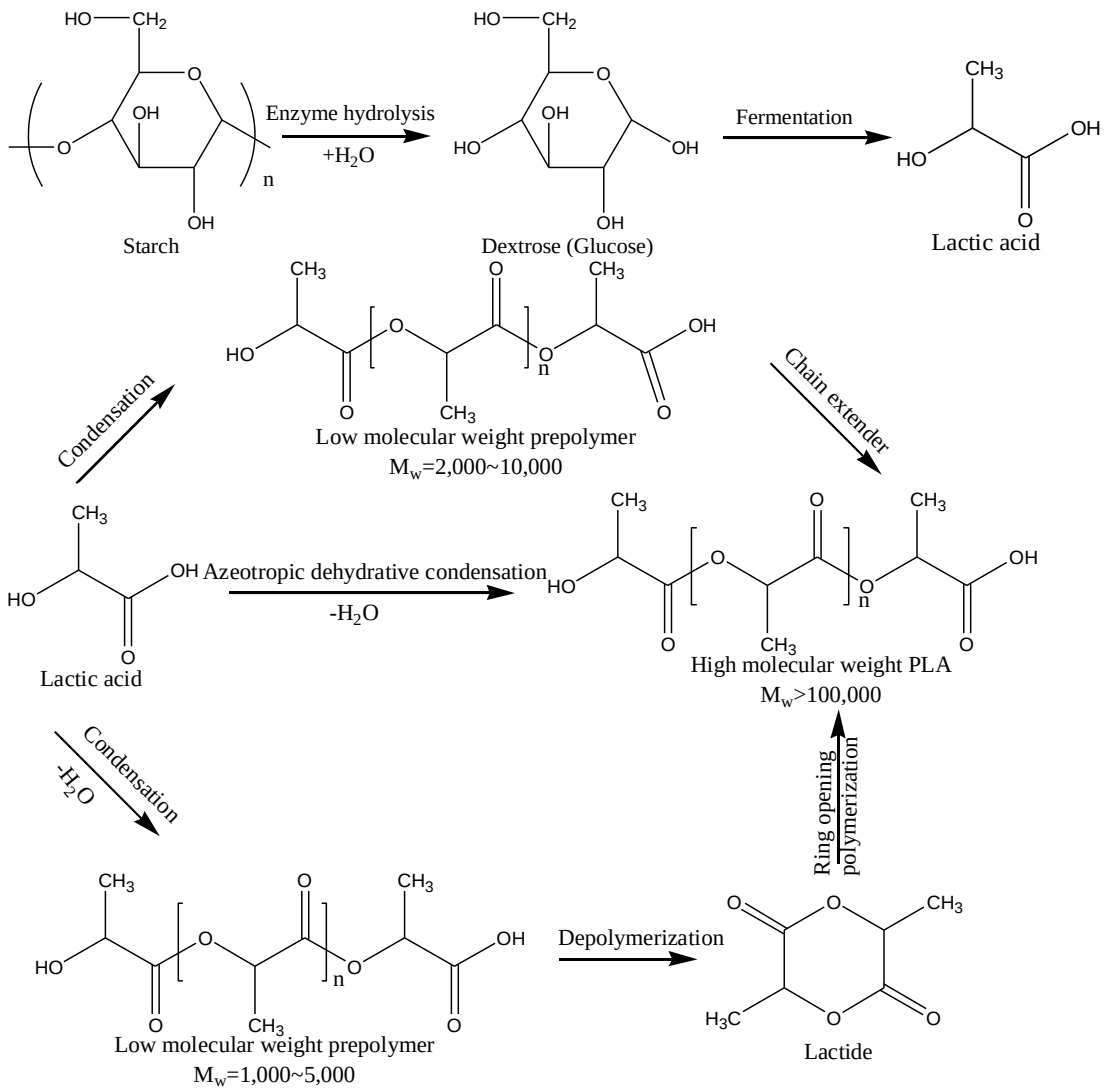

Figure 1.1. Synthesis of poly(lactic acid)

The inherent drawbacks of PLA such as poor impact strength, low elongation at break, poor melt strength, low heat deflection temperature (HDT), poor processability (high mold temperature needed for crystallization result in long cycle time for injection molding) and low thermal stability are impeding its large scale commercial application. Therefore modification in these properties of PLA is necessary for developing it as a commodity plastic in future.

1.3 Effects of various nucleating agents on PLA crystallization

Crystallization behaviors such as crystallization kinetics, crystal structure and arrangement of crystallites have a profound effect on the physical and mechanical properties of biodegradable polymers (Maiti et al., 2002; Gagnon et al., 1992; Tang et al., 2011; Shi et al., 2012); therefore, study of crystallization behaviors of PLA is of great importance because crystallization influences not only the crystal structure of PLA but also the final physical and mechanical properties of PLA products.

The crystallinity and crystallization rate of semicrystalline polymers can be enhanced through the presence of nucleating agent (NA) because the NAs improves the nuclei generation of these polymers (Kawamoto et al., 2003). Thus, the use of suitable nucleating agents is believed to be an effective method to resolve the issue concerning the low crystallization rate of PLA in practical application.

1.3.1 Inorganic nucleating agent

Most of the nucleating agents reported for PLA are inorganic materials, such as talc, montmorillonite, SiO_2, $CaCO_3$, etc. Talc is a widely used nucleating agent. Talc has been known to nucleate poly(ethylene terephthalate) for a long time. It was shown that talc nucleates the crystallization of polymers through an epitaxial mechanism (Haubruge et al., 2003). In the case of PLA, it is shown that the crystallization half-time can be reduced by more than one order of magnitude to less than 1 min when 1% talc is added (Ke et al., 2003). Battegazzore et al. reported that the incorporation of talc in PLA not only accelerated the crystallization rate of PLA but

also improved the thermal and mechanical properties of PLA. Moreover, the crystallization rate increased slightly as the talc content in the PLA/talc blends increased (Battegazzore et al., 2011). It was indicated that the crystallinity of PLA/montmorillonite (MMT) nanocomposites increased remarkably at the MMT loadings higher than 5 wt%, and the crystallization behavior of PLA was altered significantly in the presence of MMT (Ublekov et al., 2012). Buzarovska stated that the degree of crystallinity (Xc) of the PLA/TiO_2 films was increased with the increase of TiO_2 content (up to 5 wt% of TiO_2) (Buzarovska et al., 2012). After blending PLA with a little amount of nucleating agents of $CaCO_3$, TiO_2 and $BaSO_4$, the crystallinity and crystallization rate of PLA increased. Moreover, nucleating agents $BaSO_4$ and TiO_2 had better effects on the crystallinity than $CaCO_3$ (Liao et al., 2007). Although inorganic nucleating agents dramatically improve the crystallization rate and crystallinity of PLA and possess better processability and lower cost, these inorganic nucleating agents likely decrease the transparency and ultimately the physical properties of PLA due to their low compatibility with PLA and easy aggregation to sub-micrometer sizes (Nakajima et al., 2010). In addition, most inorganic fillers are nondegradable and reduce the degradability of the composites.

1.3.2 Low molecular weight organic compound nucleating agent

Besides inorganic materials, many low molecular weight organic compounds such as N, N’, N’’-tricyclohexyl-1,3,5-benzenetricarboxylamide (TMC-328), triphenyl phosphate (TTP) and low molecular weight aliphatic amides can also be

used as nucleating agents to accelerate the crystallization process and increase the crystallinity of PLA (Bai et al., 2011; Xiao et al., 2010; and Xing et al., 2012). Some low molecular weight biodegradable organic nucleating agents not only enhance the crystallization behavior of PLA but also retain the degradability of PLA. Nam et al. (2006) detected that N, N'-Ethylenebis (12-hydroxystearamide) (EBH) which crystallized at very early stage of PLA crystallization acted as an effective nucleating agent to improve the crystallization of PLA. As a result, typical tanscrystallites formed at the interface between PLA and EBH, and the overall crystallization rate was increased by the addition of EBH. Harris observed that N, N'-ethylenebisstearamide (EBSA) also improved the crystallization rate of PLA as well as the crystallinity for both isothermal and nonisothermal crystallization processes (Harris et al., 2008). Xing conducted a comparison between EBSA and EBH concerning the effect on the nucleating ability and crystallization kinetics of PLA, finding that EBH showed a stronger effect than that of EBSA. The hydrogen bond interaction between hydroxyl groups in EBH and the carbonyl groups in PLA may be responsible for the stronger nucleating ability of EBH (Xing et al., 2012). However, most low molecular weight nucleating agents are either not commercially available or more expensive than inorganic and polymeric nucleating agents.

1.3.3 Polymeric nucleating agent

Polymer blending is an effective way to modify properties of polymers. Therefore, it is believed that blending with polymers with high crystallinity is a viable

method to enhance the crystallization process of semicrystalline polymers. In the case of PLA, poly($_D$-lactic acid) (PDLA), poly(butylenes succinate) (PBS), poly(ε-caprolactone) (PCL), poly(glycolic acid) (PGA), poly(propylene glycol) (PPG), etc are reported to be effective polymeric nucleating agents for PLA. Blends of isotactic poly($_L$-lactic acid) (PLLA) and poly($_D$-lactic acid) (PDLA) resulted in the formation of a 1/1 stereocomplex: the stereocomplex had a higher melting temperature (230 ^{o}C) than pure PLLA and crystallized at higher temperature from the melt (Ikada et al., 1987). These stereocomplex crystallites acted as heterogeneous nucleation sites for corresponding PLLA crystallization and were more effective than talc on improving the crystallization of PLLA (Scott et al., 2001). Yokohara et al. realized that crystallization of PLA is improved by the incorporation of poly(butylenes succinate) (PBS) even in the molten state, thus PBS acted as a nucleating agent for PLA and may be responsible for the pronounced cold crystallization of PLA/PBS blends (Yokohara et al., 2008). The presence of poly(ε-caprolactone) (PCL) in PLA was noted to accelerate the growth of crystallites and increase the number of crystallites for the PLA matrix, indicating that PCL is an effective nucleating agent for PLA crystallization (Lopez et al., 2006). Tsuji et al. presented that the addition of poly(glycolic acid) (PGA) promoted the overall crystallization of PLA during both heating and cooling processes and the causation of the enhanced crystallization is different from that of the PLA stereocomplex (Tsuji et al., 2008).Besides low molecular weight inorganic and organic compounds and polymeric nucleating agents, some other novel materials such as carbon nanotubes

can be used as nucleating agents to enhance the crystallization of PLA as well (Barrau et al., 2011).

1.4 Methods and development of enhancing heat resistance of PLA

Although PLA has many advantages such as high tensile strength and modulus, the disadvantage of low heat deflection temperature (HDT) dramatically limits its market potential. For example, the molded PLA parts could be deformed during transportation or under operation because the ambient temperature was higher than HDT of PLA (about 60 ^{o}C). Therefore, improvements in HDT must be done prior to wide engineering applications. Several efforts have been tried to improve HDT of PLA. HDT of PLA could be improved through the addition of nucleating agents such as layered silicate, talc, methacrylate-butadiene-styrene (MBS), ethylenebishydroxystearamide (EBH), etc. Nucleating agents not only decreased the crystallization time, but also increased the mechanical properties (Ray et al., 2003, Yu et al., 2012; Zhang et al., 2012; and Tang et al., 2012). However, low content of nucleating agent/fillers in PLA did not bring obvious improvements of HDT. As listed in Table 1.1, adding 50 wt% PMMA only gave 4 ^{o}C HDT improvements over the neat PLA control. To gain 14 ^{o}C improvements, 80 wt% PMMA was needed in the blends. In this circumstance, PLA was no longer the primary component and the commercial value of PLA blends as biobased materials was compromised (Zhu et al., 2009).

Table 1.1. HDT values of various PLA blends published by NatureWorks LLC.

	% Polymer in PLA Blends	HDT (^{o}C @0.455 MPa)	HDT Improvements over neat PLA (^{o}C)
Polycarbonate	20	59	0
PMMA	20	58	-1
	50	63	4
	80	73	14
ABS	20	58	-1
	50	61	2
	80	89	30
PLA	100	58	0

1.5 Research objectives

PLA is a thermoplastic biodegradable polyester synthesized from the lactic acid feedstock. Lactic acids are produced through fermentation of cornstarch, sugarcane or other renewable materials. Because of its high strength and stiffness, PLA is treated as a promising alternative to substitute conventional petroleum-based plastics in many applications. Polyoxymethylene (POM) is one of the widely used engineering thermoplastic which is highly crystalline and has very good mechanical and thermal properties such as high tensile strength, flexural modulus and heat deflection temperature (HDT). Furthermore, high creep, fatigue and corrosive resistance of POM enable it suitable for commercial applications such as gears, pump impellers,

carburetor bodies, etc. To a certain extent, PLA and POM are complementary in many aspects, because the good heat resistance and high crystallinity of POM is expected to enhance the HDT and crystallization behavior for PLA.

The ***long-term goal*** of this research is to obtain high performance PLA blends to successfully substitute conventional petroleum-based plastics in the current commercial market. Specifically, the ***overall objective*** of this study is to develop PLA/POM blends with enhanced heat resistance and illustrate the structure-property relationship. In order to achieve the objective of this research, the following two ***specific aims*** are proposed:

Specific aim 1: Investigate the effects of different fillers, talc as an inorganic nucleating agent and POM as a polymeric nucleating agent, on the crystallization behavior and crystalline morphology of PLA.

The hypothesis for this specific aim is that talc maybe more effective than POM on accelerating the crystallization process of PLA. Moreover the crystalline morphology maybe altered by the presence of POM and talc. Talc alters the spherulites to smaller size while POM results in well-defined banded spherulites.

Specific aim 2: Investigate the changes of HDT of PLA through the presence of POM, and the relationship between POM content and HDT.

The hypothesis for this specific aim is that the high content of POM will improve the HDT of PLA.

The research of this thesis is ***creative and original***; Blending PLA with POM through melt extrusion has not been reported elsewhere in the literature, and using POM as a nucleating agent to improve crystallization and resulting in higher HDT of PLA will be introduced for the first time. The expected outcomes of this research are: (1) Understanding of the influences of adding POM on the crystallization behavior i.e. crystallization rate and crystalline morphology of PLA. (2) Understanding of the structure-property relationship of PLA/POM blends. (3) Understanding of the improvement of HDT of PLA by the presence of POM.

References

Amass, W.; Amass, A., "A review of biodegradable polymers: uses, current developments in the synthesis and characterization of biodegradable polyesters, blends of biodegradable polymers and recent advances in biodegradation studies." Polymer International, (1998) 47 (2): 89-144.

Ragauskas, J.; Williams, C., "The Path Forward for Biofuels and Biomaterials." Science, (2006) 311: 484-489.

Bioplastics - Global Market Overview, New York, Jan. 4, 2012; Available from: http://www.prnewswire.com/news-releases/bioplastics---global -market-overview-136647193.html

Carole, T.; Pellegrino, J., "Opportunities in the Industrial Biobased Products Industry." Applied Biochemistry and Biotechnology, (2004) 115: 871-885.

Kurian, J., "Polymer: Present Status and future Perspectives." Natural Fibers, Biopolymers and Future Perspectives, (2005).

Drumright, R.; Gruber, P., "Polylactic Acid Technology." Advanced Materials, (2000) 12 (23): 1841-1846.

Holten, C., Lactic acid. Properties and chemistry of lactic acid and derivatives, Verlag Chemie, Germany, (1971)

Bhardwaj, R.; Mohanty, A., "Advances in the Properties of Polylactides Based Materials: A Review." Journal of Biobased Materials and Bioenergy, (2007) 1: 191-209.

Haubruge, H.; Daussin, A., "Epitaxial Nucleation of Poly(ethylene terephthalate) by Talc: Structure at the Lattice and Lamellar Scales." Macromolecules, (2003) 36: 4452-4456.

Ke, T.; Sun, X., "Melting behavior and crystallization kinetics of starch and poly(lactic acid) composites." Journal of Applied Polymer Science, (2003) 89: 1203-1210.

Battegazzore, D.; Bocchini, S., "Crystallization kinetics of poly(lactic acid)-talc composites." eXPRESS Polymer Letters, (2011) 5 (10): 849-858.

Ublekov, F.; Badrian J., "Influence of Clay Content on the Melting Behavior and

Crystal Structure of Nonisothermal Crystallized Poly(L-lactic acid)/Nanocomposites." Journal of Applied Polymer Science, (2012) 124 (2): 1643-1648.

Buzarovska, A.; Grozdanow, A., "Biodegradable Poly(L-lactic acid)/TiO_2 Nanocomposites: Thermal Properties and Degradation." Journal of Applied Polymer Science, (2012) 123 (4): 2187-2193.

Liao, R.; Yang, B., "Isothermal Cold Crystallization Kinetics of Polylactide/Nucleating Agents." Journal of Applied Polymer Science, (2007) 104: 310-317.

Bai, H.; Zhang, W., "Control of Crystal Morphology in Poly(L-lactide) by Adding Nucleating Agent." Macromolecules, (2011) 44: 1233-1237.

Xiao, H.; Li., "Isothermal Crystallization Kinetics and Crystal Structure of Poly(lactic acid): Effect of Triphenyl Phosphate and Talc." Journal of Applied Polymer Science, (2010) 118: 3558-3569.

Xing, Q.; Zhang, X., "Low-molecular weight aliphatic amides as nucleating agents for poly(L-lactic acid): Conformation variation induced crystallization enhancement." Polymer, (2012) 53: 2306-2314.

Nam, J.; Okamoto, M., "Morphology and crystallization kinetics in a mixture of low-molecular weight aliphatic and polylactide." Polymer, (2006) 47: 1340-1347.

Harris, A.; Lee, E., "Improving mechanical performance of injection molded PLA by controlling crystallinity." Journal of Applied Polymer Science, (2008) 107 (4): 2246-2255.

Ikada, Y.; Jamshidi, K., "Stereocomplex formation between enantiomeric poly(lactides)." Macromolecules, (1987) 20 (4): 904-906.

Scott, C.; Marc, A., "Polylactide Seteocomplex Crystallites as Nucleating Agents for Isotactic Polylactide." Journal of Applied Polymer Science: Part B: Polymer Physics, (2001) 39: 300-313.

Yokohara, T.; Yamaguchi, M., "Structure and properties for biomass-based polyester blends of PLA and PBS." European Polymer Journal, (2008) 44: 677-685.

Lopez-Rodriguez, A., "Crystallization, morphology, and mechanical behavior of polylactide/poly(ε-caprolactone) blends." Polymer Engineering & Science, (2006) 46 (9): 1299-1308.

Tsuji, H.; Tashiro, K., "Polyglycolide as a Biodegradable Nucleating Agent for

Poly(L-lactide).” Macromolecular Materials and Engineering, (2008) 293: 947-951.

Barrau, S.; Vanmansart, C., “Crystallization Behavior of Carbon Nanotube - Polylactide Nanocomposites.” Macromolecules, (2011) 44 (16): 6496-6502.

Ray, S.; Yamada, K., “New polylactide-layered silicate nanocomposites. 2. Concurrent improvements of material properties, biodegradability and melt rheology.” Polymer, (2003) 44: 857-866.

Yu, F.; Liu, T., “Effects of Talc on the Mechanical and Thermal Properties of Polylactide.” Journal of Applied Polymer Science, (2012) 125 (S2): E99-E109.

Zhang, H.; Liu, N., “Toughening of Polylactide by Melt Blending with Methyl Methacrylate-Butadiene-Styrene Copolymer.” Journal of Applied Polymer Science, (2012) 125 (S2): E550-E561.

Tang, Z.; Zhang, C., “The crystallization Behavior and Mechanical Properties of Polylactic Acid in the Presence of a Crystal Nucleating Agent.” Journal of Applied Polymer Science, (2012) 125 (2): 1108-1115.

Zhu, S., “PLA property improvement: Improving the practical heat resistance of Polylactic Acid (PLA).” 2009.

Chapter 2 Crystallization and morphology of PLA Blends

Abstract

In this work, crystallizations of neat poly(lactic acid) (PLA) and PLA in the presence of small portion of polyoxymethylene (POM) were investigated by differential scanning calorimetry (DSC), polarized optical microscope (POM) and X-ray diffraction (XRD) in detail for a comparative study of the effects of different fillers on the morphology and crystallization of PLA. For comparison, PLA crystallization in the presence of small amount of talc was also studied. Interpretation of the results suggest that the crystal structure of PLA was changed by the additions of POM and talc, and the crystallization ability of PLA was enhanced in both cases. Talc was found to be more efficient than POM in enhancing the crystallization of PLA. The PLA/POM exhibited higher transmittance than neat PLA and the PLA/talc, indicating POM was miscible or semi-miscible with PLA. This result was consistent with the FTIR results. In addition, well-defined banded spherulites were found in the PLA/POM blends during isothermal crystallization.

Keywords: crystallization kinetics, crystalline morphology, transparency, crystal structure, miscibility

2.1 Introduction

As a biodegradable aliphatic polyester, PLA has attracted increasingly attention in recent years due to its excellent mechanical properties, biodegradability and potential renewability. However, there is a critical issue concerning the low crystallization rate of PLA. Despite the fact that PLA is a semicrystalline polymer, almost no crystallization proceeds under fast cooling such as a practical molding condition (Kawamoto et al., 2007). The low crystallization rate of PLA results in poor heat resistance, processability and productivity (Defosse et al., 2005) and severely limits the range of application of PLA.

In general, it is known that nucleating agents (NA) enhance the nuclei generation in semicrystalline polymers during crystallization process and leads to higher crystallization rate at higher temperature, resulting in increased crystallinity (Kawamoto et al., 2003; Funamizu et al., 2005). Therefore, the utilization of suitable nucleating agents is believed to be one of the solutions for the low crystallization rates of PLA in practical application. Some inorganic compounds such as talc and zinc phenylphosphonate (PPA-Zn) have been utilized for improving the crystallinity of PLA. However, if an uniform nano-scale dispersion in the matrix is not achieved, these inorganic compound, will likely decrease the transparency of PLA due to the light scattering by the large particles. For this reason, organic crystal nucleators with good compatibility are preferably used for enhancing the crystallization of PLA. It has been reported that methylenebis(2,4-di-tert-butylphenyl)phosphate sodium salt (NA-11) commercialized as nulceator for PP can also enhance crystallization of PLA

(Kawamoto et al., 2007). In this study, polyoxymethylene (POM) as a polymeric nucleating agent was introduced to enhance the crystallization of PLA because the regular structure (typical helical chain structure with a sequence of gauche C-O bonds) of POM causes polymers to crystallize easily and to form large spherullites in the melting processing.

Crystallization behaviors play an important role in affecting the physical and thermal properties of biodegradable polymers (Maiti et al., 2002; Gagnon et al., 1992; Tang et al., 2011; Shi et al., 2012); therefore, the crystallization kinetics study is of great importance because it influences not only the crystalline structure and morphology of semicrystalline polymers but also the final physical and thermal properties of biodegradable polymers. The presence of fillers usually has the following complicated effects on the crystallization of the polymer matrix: acceleration/retardation of crystallization, changes in the spherulitic morphology, and modification in the crystal structure in a few cases. The aim of this work is to conduct a comparative study of the influences, POM (polymeric nucleating agent) and talc (inorganic nucleating agent), on the crystallization behavior and morphology of PLA for a better understanding of the crystallization behavior of polymers in polymer blends.

2.2 Experimental

2.2.1 Materials

All the materials used in this study are listed in table 2.1.

Table 2.1. Characteristics of materials used in this study

Materials (abbreviation)	Grade (supplier)	Specifications
Poly(lactic acid) (PLA)	PLA 2002D (NatureWorks)	MI(201°C, 2.16kg) = 5~7g/10min Specific Gravity = 1.24
Polyoxymethylene (POM)	RTP 800 (RTP Co.)	Specific Gravity = 1.41
talc	Magsil 3183A (RBH Co.)	Specific Gravity = 2.75

All materials in this study were used as received without further purification.

2.2.2 Preparation of neat PLA and PLA blends with POM and talc

Prior to extrusion, pellets of PLA and POM, and talc powder were dried at least 1 day at 85 ^{o}C in an oven to remove any moisture present in the sample. The PLA and the fillers were premixed manually through tumbling in a sealed plastic bag. A co-rotating twin-screw extruder (Leistritz ZSE-18) equipped with a volumetric feeder and a pelletizer was used to prepare the PLA/POM blends. The screw diameter and L/D ratio of the extruder were 17.8 mm and 40, respectively. The screw speed was

maintained at 50 rpm for all runs, and the temperature profile of the barrel was (160, 160, 200, 200, 200, 170, 150 and 150 ^{o}C) from the first heating zone (next to the feeding throat) to the die. The extrudate was cooled under water and subsequently granulated. Blend compositions (in wt%) of the PLA/POM blends were 99/1, 98/2 and 95/5. Neat PLA and the PLA/talc blends (PLA/talc=99/1, 98/2 and 95/5 in wt%) were prepared under the same conditions. Before injection molding, the blends were dried at 85 ^{o}C for 1 day in a convection oven. Standard tensile (ASTM D638, Type I) test specimens were prepared using injection molding (Sumitomo SE 50D) at melt temperature of 190 ^{o}C and mold temperature of 40 ^{o}C. After injection molding, all specimens were conditioned at 23 ^{o}C and 50% RH for 7 days prior to characterization. The blends with 1, 2 and 5 wt% of POM are denoted as POM1, POM2 and POM5 hereafter.

2.2.3 Characterization

Differential Scanning Calorimetry (DSC). Crystallization of the PLA/POM blends were studied using differential scanning calorimeter (Mettler Toledo, DSC 822e). Sample ca. 5 mg were crimp sealed in 40-μL aluminum pans, each sample was tested in duplicates. To determine the crystallization and melting temperatures, the samples were first heated up to 200 ^{o}C at 10 ^{o}C/min and held isothermally for 5 min to erase the thermal history, then cooled to 0 ^{o}C at 10 ^{o}C/min, and finally heated up to 200 ^{o}C at the same rate. The isothermal crystallization was carried out with the same DSC

instrument. The samples were first heated up to 200 ^{o}C at 10 ^{o}C/min and held isothermally for 5 min to erase the thermal history, then cooled to the predetermined crystallization temperatures (106, 107, 108, 109 and 111 ^{o}C) at the cooling rate of 80 ^{o}C/min and held isothermally for 30 or 15 min depending on when the exothermic peak appeared. For nonisothermal crystallization, the samples were first heated up to 200 ^{o}C and held isothermally for 5 min to erase thermal history, then cooled to 25 ^{o}C at different cooling rates of 5, 10, 20, 30 and 40 ^{o}C/min. The exotherms of isothermal and nonisothermal crystallization were recorded for analysis.

Polarized Optical Microscopy. Spherulitic crystal growth and morphology was observed using a polarized optical microscope (Olympus BX51) equipped with a hot stage (Linklam TMS 94). Thin film samples were prepared by melting the blends between microscope cover slips. The samples were first heated up to 200 ^{o}C at 50 ^{o}C/min and held at 200 ^{o}C for 3 min to erase previous thermal history and press the blends into thin film, then quenched to the designed isothermal crystallization temperature (130 ^{o}C) to observe the spherulitic growth and morphology of the blends and their components.

UV-Visible Spectrometry (UV-vis). The optical transmittances of neat PLA and its two blends with POM and talc were measured at wavelength from 200 to 1100 nm using a UV-vis spectrophotometer (Evolution 300, Thermo Scientific). Transmittance

spectra were measured using air as a reference. The sheets used for characterization were prepared by melting and then quickly quenching into a thickness of ~100 μm between two steel plates.

Fourier Transform Infrared Spectroscopy (FT-IR). The absorption spectra were recorded using a Thermo Nicolet Nexus 670 spectrometer (Nicolet, Thermo Scientific) with a resolution of 4 cm^{-1} and 32 scans and a Smart iTR (Thermo Scientific) with a pointed pressure tip and a crystal plate of Ge crystal. The sheets of neat PLA and its blends with POM used for characterization were prepared by melting and then quickly quenching to room temperature.

Wide angle X-ray diffraction (WAXD). XRD patterns were recorded using a X-ray diffractometer (Empyrean, PANalytical). The CuKα radiation (λ = 0.15418 nm) source was operated at 40 kV and 40 mA. The sheets of neat PLA and its two blends with POM and talc used for characterization were prepared by melting and then quickly quenching to room temperature into a thickness of around 100 μm. XRD patterns were recorded from 5 to 90° at 8°/min.

Scanning electron microscopy (SEM). Cryo-fractured surfaces of neat PLA and PLA blends samples were examined using a Quanta 200F field emission scanning electron microscope (FE-SEM, FEI Co.) at an accelerated voltage of 15 kV. All specimens were sputter-coated with gold prior to examination.

Mechanical test. Tensile tests were conducted on a universal testing machine (Instron 4466) following ASTM D638 (type I specimens). The crosshead speed was 0.2 in/min (5.08 mm/min) for all the specimens, and the initial strain was measured using a 2 in (50.8 mm) extensometer. Notched Izod impact tests were performed according to ASTM D256 using a BPI-0-1 Basic Pendulum Impact tester (Dynisco, MA). Average value of five replicates were taken for each sample.

2.3 Results and discussion

2.3.1 Crystallization behaviors of neat PLA and PLA blends

The first heating curves of neat PLA and PLA/POM bends are shown in Figure 2.1. The DSC parameters of the heating process are summarized in Table 2.2. The glass transition temperature (T_g) of PLA in all samples was around 55 ^{o}C. The PLA displayed a cold crystallization exotherm that varied with POM content and was denoted as cold crystallization temperature. Comparing neat PLA with the PLA/POM blends, the presence of 5 wt% POM decreased the cold crystallization temperature from 110 to 102.3 ^{o}C and narrowed the exothermic peak width, indicating an enhancement in crystallization of PLA. In addition, two cold crystallization exothermic peaks were observed in the POM1, POM2 and POM5 curves. The exothermic peaks around 100 ^{o}C of neat PLA and PLA/POM blends were assigned to the cold crystallization of PLA due to the low crystallization rate of PLA during

molding process. The smaller exothermic peaks around 80 ^{o}C of PLA/POM blends might be induced by the presence of POM. A possible explanation for this was the high cooling rate during the molding process and the interfacial reactions between PLA and POM which resulted in the incompleteness and retard of crystallization of POM in the blends. The PLA/POM blends exhibited a higher enthalpy of cold crystallization (ΔH_c) than neat PLA, which also confirmed that the incorporation of POM improved the crystallization ability of PLA. In the first heating scan, the difference between enthalpy of melting and enthalpy of cold crystallization (ΔH_m-ΔH_c) was the true enthalpy of fusion of the PLA crystals in the original molded sample. For POM1, POM2 and POM5, the values of (ΔH_m-ΔH_c) were 1.99, 2.84 and 6.7 J/g, respectively, which were much greater than the value (0.58 J/g) for the neat PLA. The very similar values of ΔH_m and ΔH_c for neat PLA indicated that neat PLA sample was mainly amorphous. Therefore, the addition of POM greatly increased the crystallization rate of PLA.

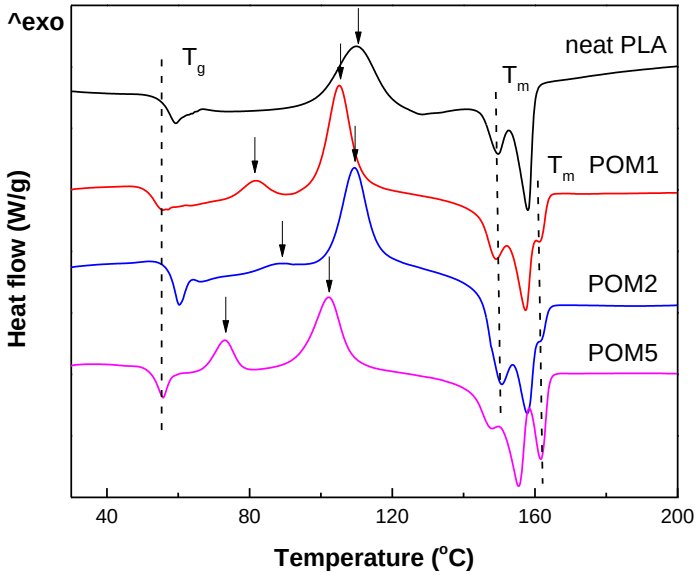

Figure 2.1. First heating DSC curves of neat PLA, POM and the PLA/POM blends

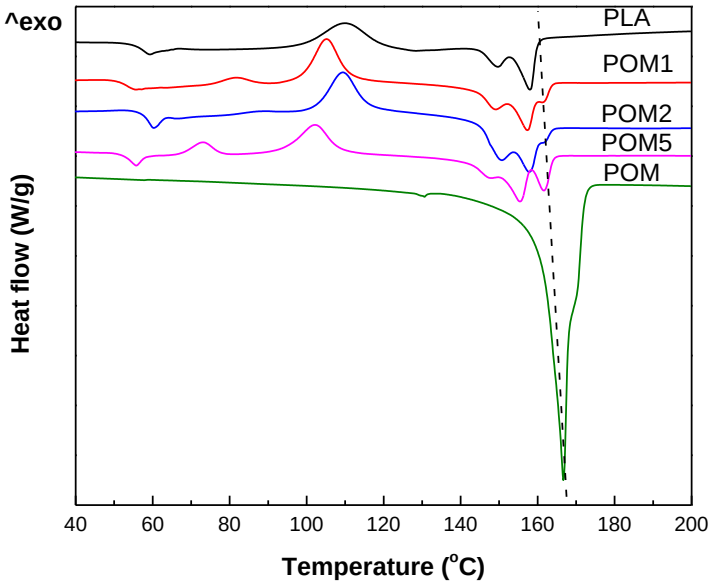

Figure 2.2 First heating DSC curves of neat PLA, POM and the PLA/POM blends

Table 2.2. DSC parameters of melting and crystallization for neat PLA, POM and the PLA/POM blends

Sample	T_g	T_{cc}		ΔH_c	ΔH_m	ΔH_m-ΔH_c
	^{o} C	^{o} C		J/g	J/g	J/g
PLA	56.5	n.a.	110	20.83	21.41	0.58
POM1	52.7	81.5	105.2	26.76	28.75	1.99
POM2	57.4	88.5	108.3	26.34	29.18	2.84
POM5	53.4	73	102.3	26.15	32.85	6.7
POM	n.a.	n.a.	n.a.	n.a.	144.54	n.a.

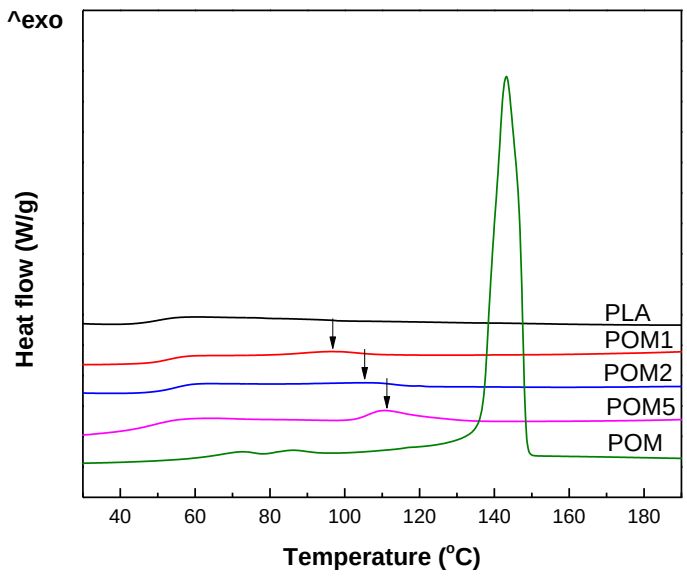

Figure 2.3. First cooling DSC curves of neat PLA, POM and the PLA/POM blends

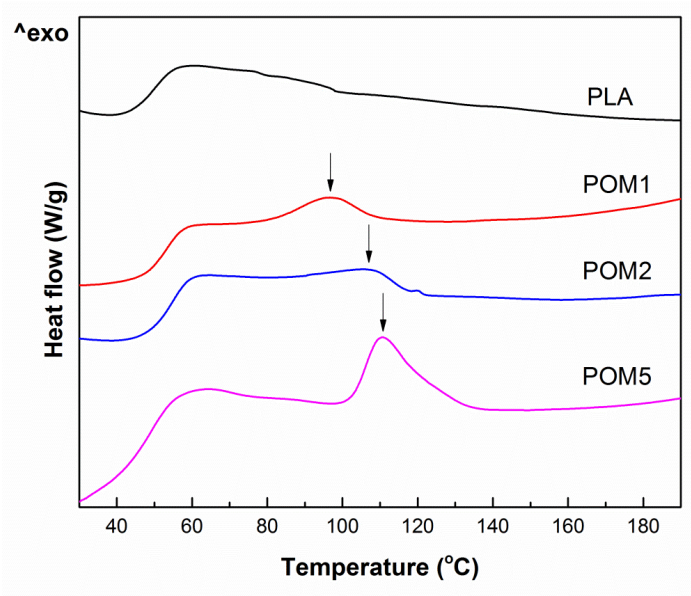

Figure 2.4. First cooling curves of neat PLA and PLA/POM blends

Table 2.3. DSC parameters of cooling and crystallization for neat PLA, POM and the PLA/POM blends

Sample	T_{mc}	$\Delta H_{m,c}$	X_c
	°C	J/g	%
Neat PLA	n.a.	n.a.	n.a.
POM1	96.7	2.6	2.8
POM2	107.5	2.7	2.9
POM5	110.7	7.5	8.4
POM	143.2	152.22	n.a.

Figure 2.4 displays the thermograms from the first cooling scan of neat PLA and PLA/POM bends. The DSC results from the first cooling scan are listed in Table 2.3. Compared to neat PLA, obvious exotherms were observed during the cooling process for PLA/POM blends. The melt crystallization temperature shifted to a higher value (from 96.7 to 110.7 ^{o}C) with the POM content increasing from 1 to 5 wt%, and the enthalpy of the melt crystallization increased with increasing POM content as well. No exotherm was noted for neat PLA during the cooling. The crystallization of PLA and POM couldn't be separated in the case of POM5, for POM1 and POM2 the contribution of POM in crystallization might be ignored due to the low content of POM. Therefore, estimates of crystallinity of PLA/POM blends were obtained through equation 2.1. The crystallinity of POM1, POM2 and POM5 were 2.8, 2.9 and 8.4%, respectively. In general, the crystallization of PLA was improved by adding POM in the blends.

$$\chi_c = \frac{\Delta H_m}{W_f \times \Delta H_m^{\infty}} \times 100\% \qquad 2.1$$

Where ΔH_m is the enthalpy of melting crystallization during cooling scan; ΔH_m^{∞} is the enthalpy assuming 100% crystalline PLA (93.7 J/g) (Garlotta et al., 2011), and W_f is the weight fraction of PLA component in the blends.

Figure 2.5 displayed the thermograms from the second heating scan of neat PLA, POM and PLA/POM blends. There was only one cold crystallization exothermic peak for PLA/POM blends during second heating scan, which was ascribed to the cold crystallization peak of PLA at 110 ^{o}C.

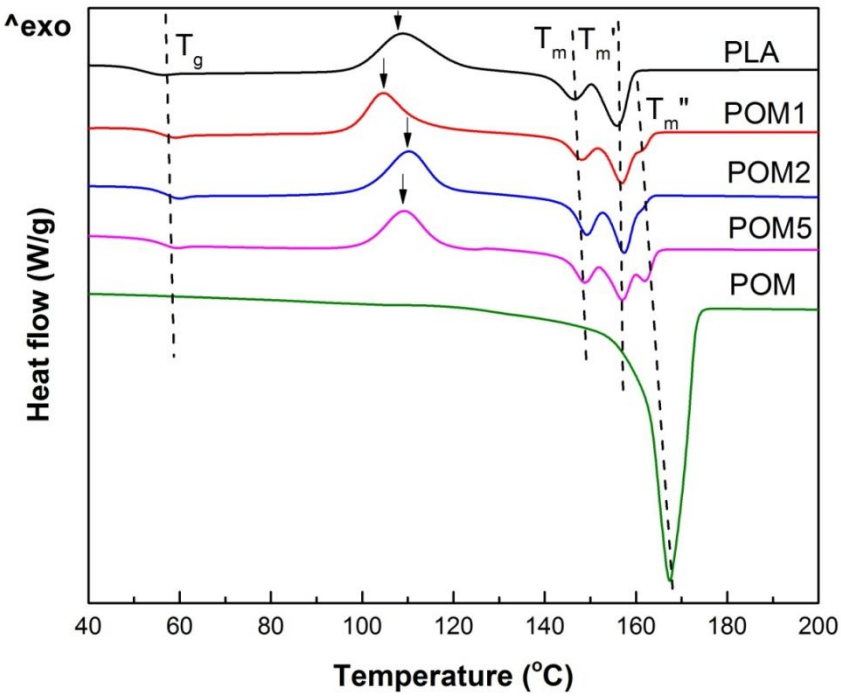

Figure 2.5. Second heating of neat PLA, POM and the PLA/POM blends

2.3.2 Crystallization Kinetics of neat PLA and PLA blends

2.3.2.1 Isothermal crystallization of neat PLA and PLA blends

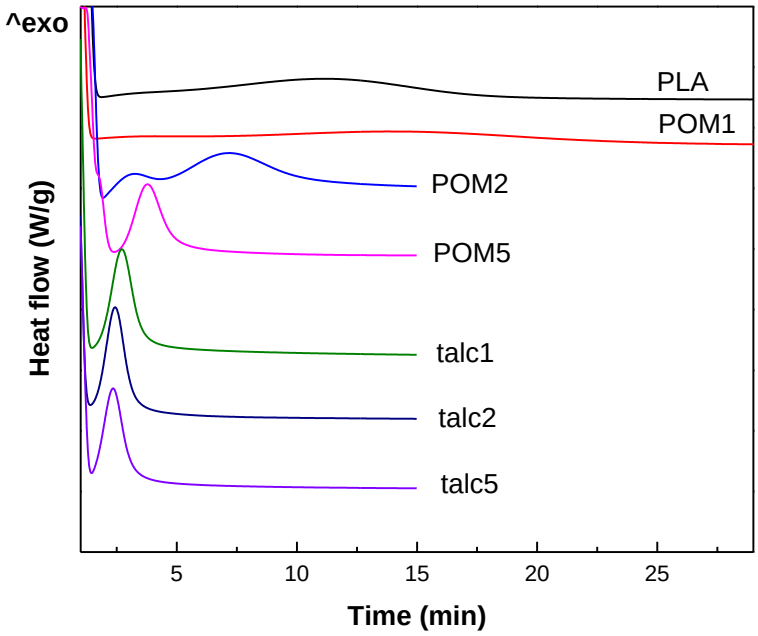

Figure 2.6. Crystallization isotherms of neat PLA, PLA/POM blends and PLA/talc blends at 108 ^{o}C. The curves were vertically shifted for legibility

Crystallization isotherms were performed by DSC to determine the crystallization duration at 108 ^{o}C. As shown in Figure 2.6, the crystallization peak time of neat PLA was observed at 11.15 min. The isotherm of POM1 displays a broader peak at 14 min, which means 1 wt% of POM hinders the crystallization of PLA. The crystallization peaks shifted to the left of neat PLA when adding more POM, indicating that the crystallization rate of PLA was improved by the presence of POM more than 1 wt%. Compared to the isotherm of neat PLA, the isotherms of talc1, talc2 and talc5 show extremely sharp and intense crystallization peaks. As a result, we

can draw the conclusion that talc is more efficient than POM in increasing the crystallization rate of PLA.

The overall isothermal crystallization kinetics of neat PLA and its two kinds of blends were further studied using DSC. In order to compare all samples under the same temperature conditions, the range of isothermal crystallization temperature for the kinetics study was limited to 106 - 111 ^{o}C. The exotherms for the melt crystallization of all samples were shown in Figure 2.7. The exothermic peak of neat PLA became flat and shifted to longer time with increasing crystallization temperature, the same pattern was found for the PLA/POM blends. This result implies that neat PLA and PLA/POM blends (POM1, POM2 and POM5) at higher crystallization temperature need longer time to complete crystallization. The pattern of crystallization of neat PLA could not be found in the PLA/talc blends. This phenomenon corresponds to a compromise between nucleation and growth of crystals: crystal nucleation is favored at low temperature when molecular mobility is low, nevertheless crystal growth is favored at high temperature when viscosity is low.

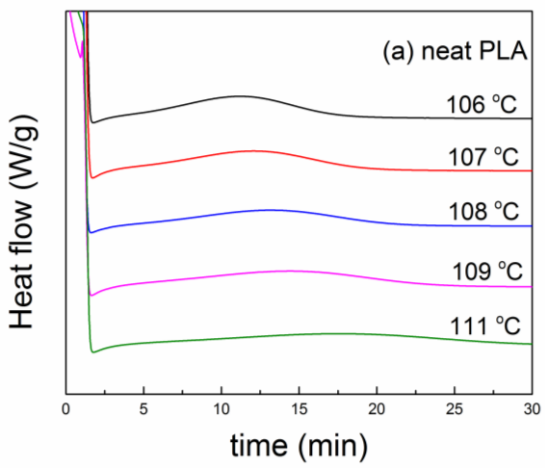
(a) neat PLA
106 °C
107 °C
108 °C
109 °C
111 °C
Heat flow (W/g)
time (min)
0
5
10
15
20
25
30

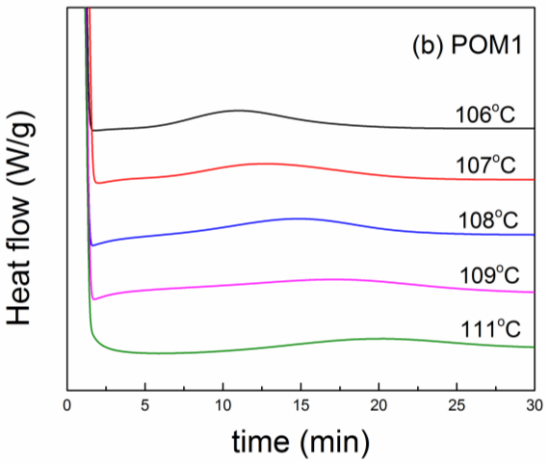
(b) POM1
106°C
107°C
108°C
109°C
111°C
Heat flow (W/g)
time (min)
0
5
10
15
20
25
30

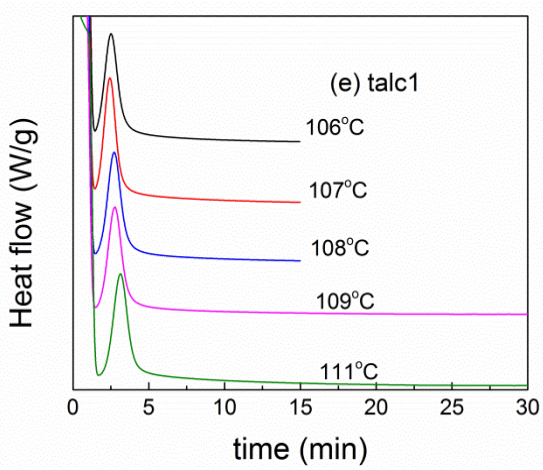
(e) talc1
106°C
107°C
108°C
109°C
111°C
Heat flow (W/g)
time (min)
0
5
10
15
20
25
30

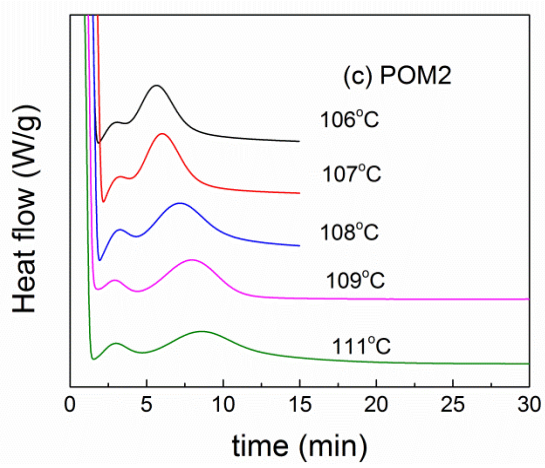
(c) POM2
106°C
107°C
108°C
109°C
111°C
Heat flow (W/g)
time (min)
0
5
10
15
20
25
30

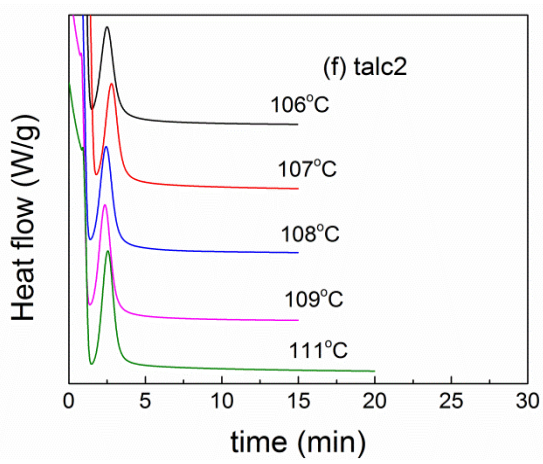
(f) talc2
106°C
107°C
108°C
109°C
111°C
Heat flow (W/g)
time (min)
0
5
10
15
20
25
30

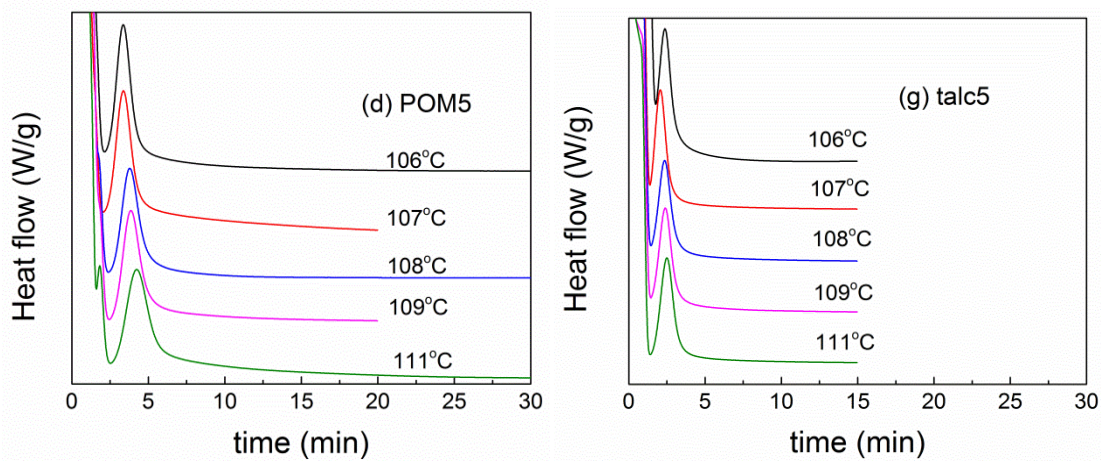

Figure 2.7. Curves of heat flow versus time for the isothermal crystallization of neat PLA, PLA/POM blends and PLA/talc blends

The plots of relative crystallinity versus crystallization time for neat PLA and its blends with POM and talc are provided in Figure 2.8. The relative crystallinity at time t, X(t), was calculated through the following equation:

$$X(t) = \frac{\int_0^t \frac{dH}{dt} dt}{\int_0^\infty \frac{dH}{dt} dt} = \frac{\Delta H_t}{\Delta H_\infty} \qquad 2.2$$

where dH/dt is the rate of heat evolution; ΔH_t is the heat generated at time t; and ΔH_∞ is the total heat generated up to the crystallization process.

The curves shown in Figure 2.8 display a sigmoid dependence on time. Generally, the isothermal crystallization process is divided into two sections: the primary crystallization stage and the secondary crystallization stage. The primary

crystallization stage for all samples shows an obvious increase in the relative crystallinity, whereas the secondary crystallization stage only provides a slight increase in the relative crystallinity.

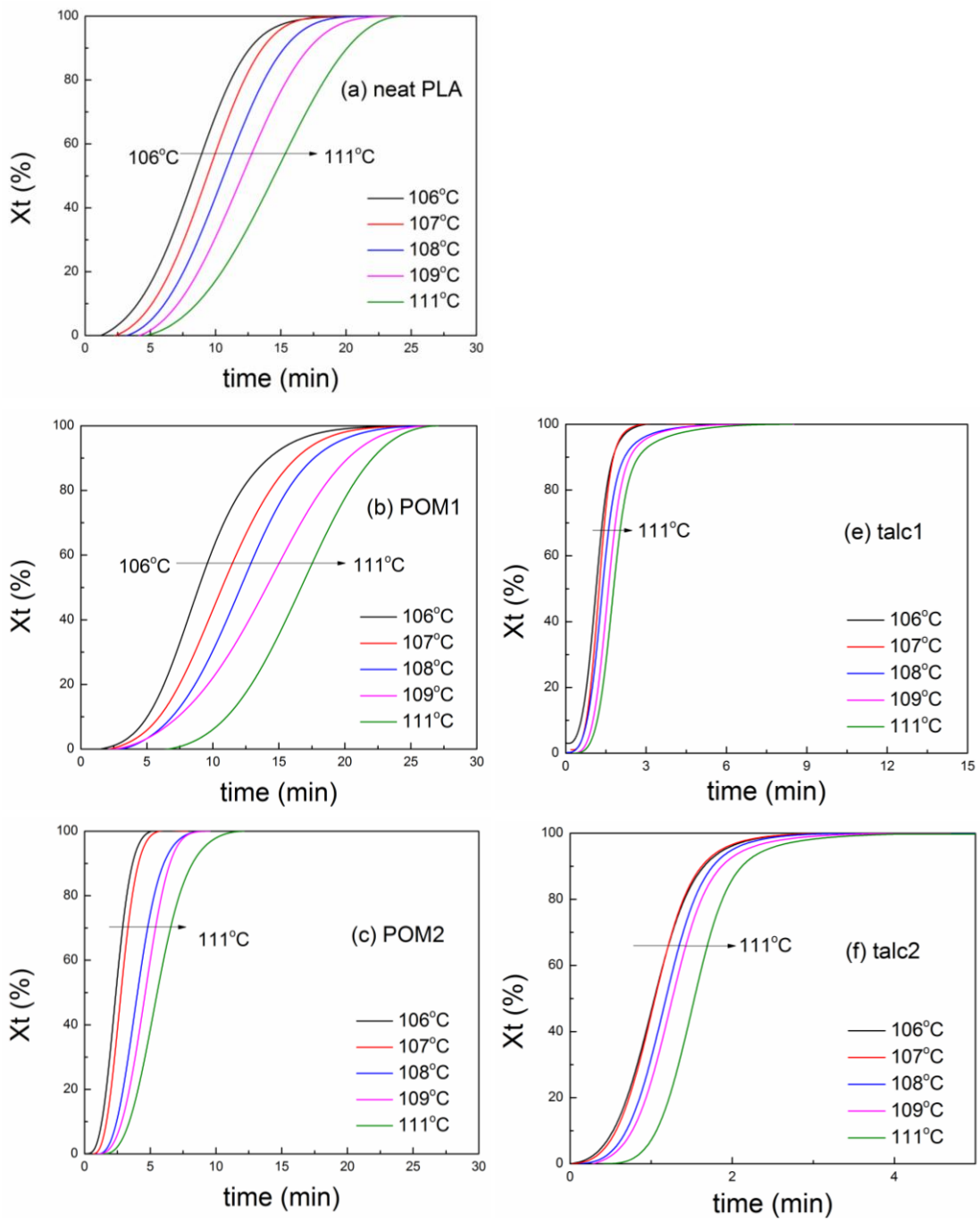

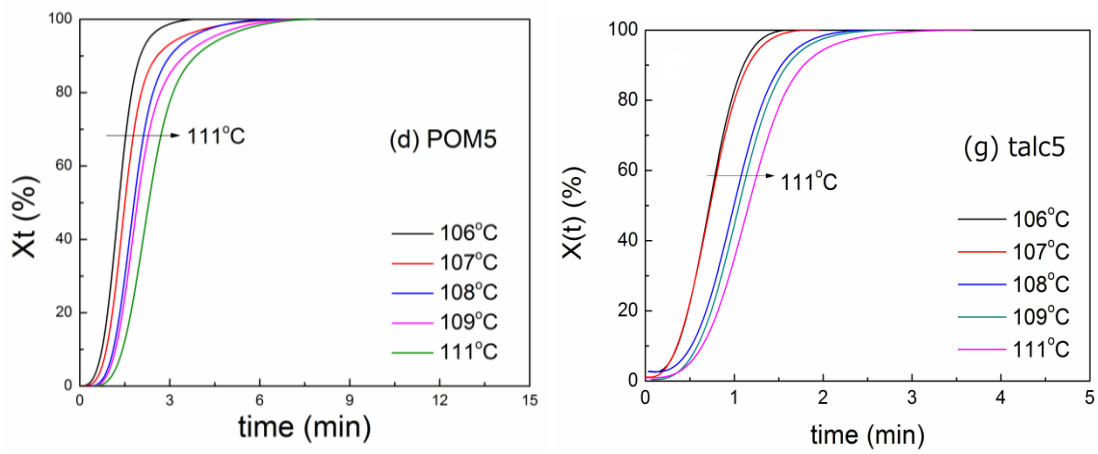

Figure 2.8. Curves of relative crystallinity versus time for isothermal crystallization of neat PLA, PLA/POM blends and PLA/talc blends

Further analysis of isothermal crystallization kinetics for neat PLA and its blends with POM and talc were conducted using the well-known Avrami's equation. It is assumed that the relative crystallinity increases with increasing crystallization time as follows:

$$X(t) = 1 - \exp(-Kt^n)$$

$$\log\{-\ln[1 - X(t)]\} = n\log t + \log K \qquad 2.3$$

where n is the Avrami exponent dependent on the mechanism of nucleation and the crystal growth dimension; K is the isothermal crystallization rate parameter.

The plots of log{-ln[1-X(t)]} versus log t for neat PLA and its blends with POM and talc were shown in Fig.9. For neat PLA and POM1, the values of n for the secondary crystallization stage are greater than those of the primary crystallization stage as shown in Table 2.2. However, the curves of POM2, POM5 and all PLA/talc blends showed an initial linear portion, and subsequently tended to deflect from the linear trend. The deviation is probably attributed to the secondary crystallization,

which was caused by the spherulite impingement in the later stage of crystallization at longer crstallization time (Wunderlich et al., 1977; Liu et al., 1997; and Dell'erba et al., 2001).

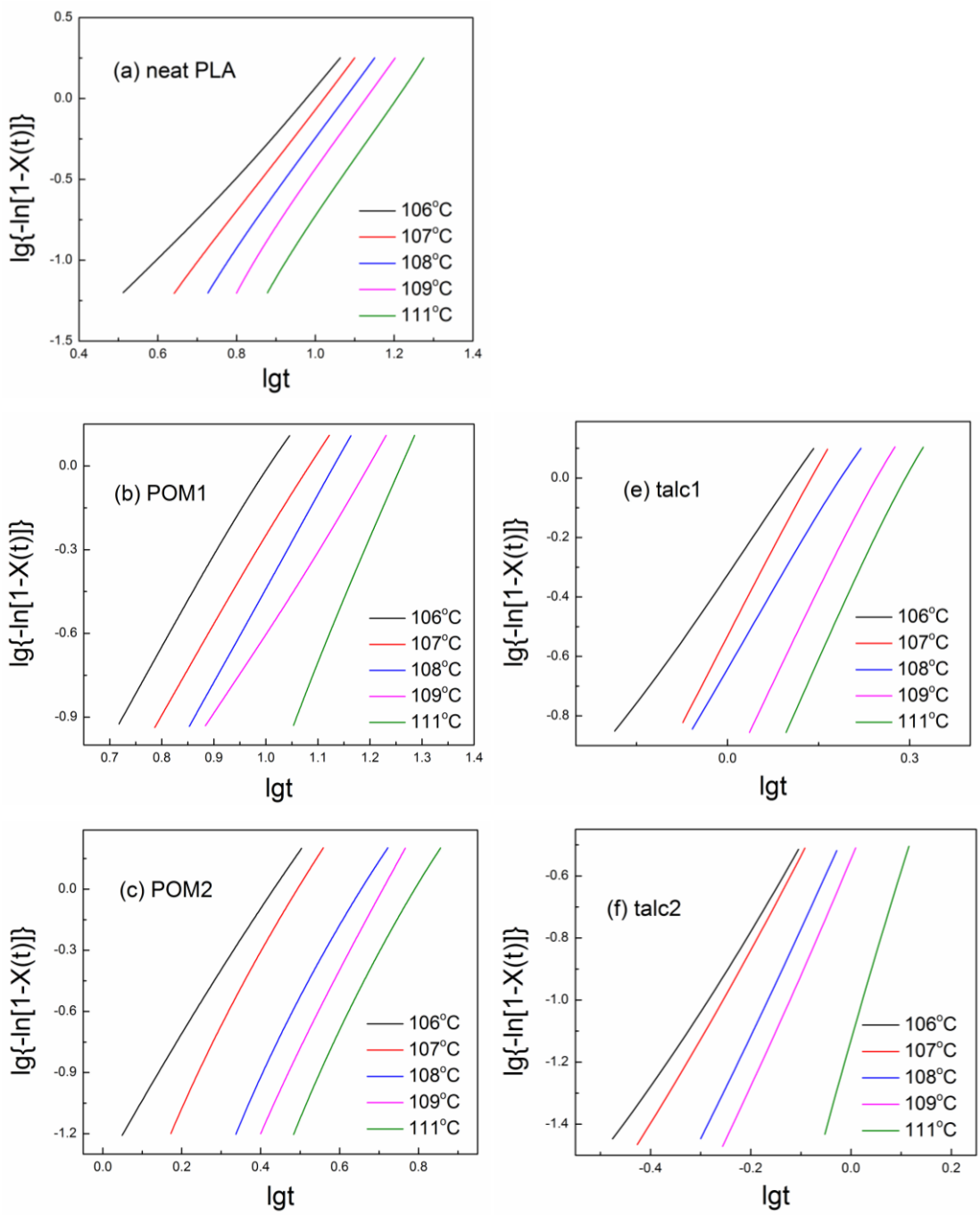

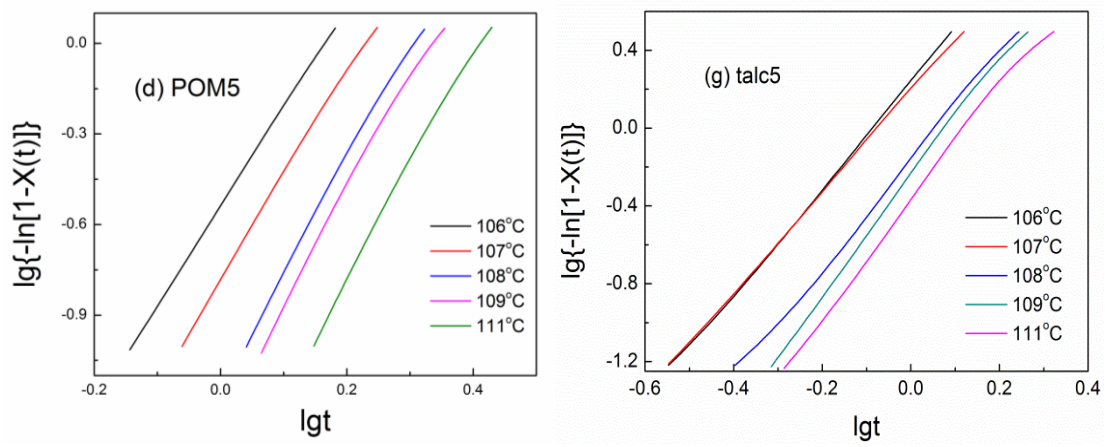

Figure 2.9. Curves of log{-ln[1-X(t)]} versus log t for isothermal crystallization of neat PLA, PLA/POM blends and PLA/talc blends

Table 2.4. Isothermal crystallization kinetics parameters for neat PLA and its two blends of POM and talc on the Avrami equation

Sample	T_C (°C)	n	K (min^{-n}) $\times 10^{-3}$	$t_{1/2}$ (min)	$T_{1/2}$ (min^{-1})
Neat PLA	106	2.66	2.5003	8.2862	0.1207
	107	3.148	0.607	9.3603	0.1068
	108	3.37	0.24044	10.633	0.094
	109	3.514	0.1089	12.091	0.0827
	111	3.568	0.04989	14.491	0.06901
POM1	106	3.1684	0.5238	9.6658	0.1034
	107	3.1256	0.4012	10.859	0.0921
	108	3.3645	0.1684	11.866	0.0843
	109	3.0013	0.1581	16.347	0.0612
	111	3.8783	0.0115	17.076	0.0586

Table 2.4. continued

POM2	106	3.0773	46.806	2.4009	0.4165
	107	3.5606	17.713	2.8007	0.3571
	108	3.5736	4.5973	4.0697	0.2452
	109	3.7687	2.138	4.6369	0.2157
	111	3.7082	1.1749	5.5875	0.179
POM5	106	3.2986	289.068	1.3036	0.7671
	107	3.4439	166.725	1.5125	0.6612
	108	3.7475	74.302	1.8146	0.5511
	109	3.7218	59.429	1.9348	0.5168
	111	3.7513	29.923	2.3111	0.4327
talc1	106	2.9483	477.64	1.1346	0.8813
	107	3.8724	294.103	1.2478	0.8014
	108	3.4374	229.774.	1.3788	0.7253
	109	3.8769	103.276	1.6341	0.612
	111	3.9216	56.208	1.8976	0.527
talc2	106	2.5317	578.762	1.0738	0.9312
	107	2.8669	549.794	1.0842	0.9224
	108	3.4295	384.769	1.1872	0.8423
	109	3.6295	286.946	1.2751	0.7843
	111	3.9889	74.08	1.7517	0.5709
talc5	106	2.647	1.7378	0.71563	1.39738
	107	2.51	1.574	0.73035	1.3692
	108	2.716	0.692	1.00067	0.99933
	109	2.934	0.5649	1.06974	0.93481
	111	2.85	0.4207	1.1844	0.84431

From the slope and intercept of the initial linear portion in Figure 2.9, the values of n and K were determined and listed in Table 2.4. The Avrami exponent n varied from 2 to 4, and this reflected the mechanism of nucleation and the crystal growth. The average value of n was around 3.2, 3.3, 3.5, 3.6, 3.6, 3.3 and 2.7 for neat PLA, POM1, POM2, POM5, talc1, talc2 and talc5, respectively. For neat PLA without heterogeneous nucleus, the crystallization followed homogeneous nucleation and spherulitic three-dimension growth from instantaneous nuclei. For PLA/POM blends and PLA/talc blends, the nucleation type is mostly heterogeneous nucleation and the spherulitic growth is three-dimensional growth from instantaneous nuclei (Sperling et al., 2006). The values of the crystallization rate parameter K for all samples increased with decreasing crystallization temperature T_c, which displayed a very different temperature dependency.

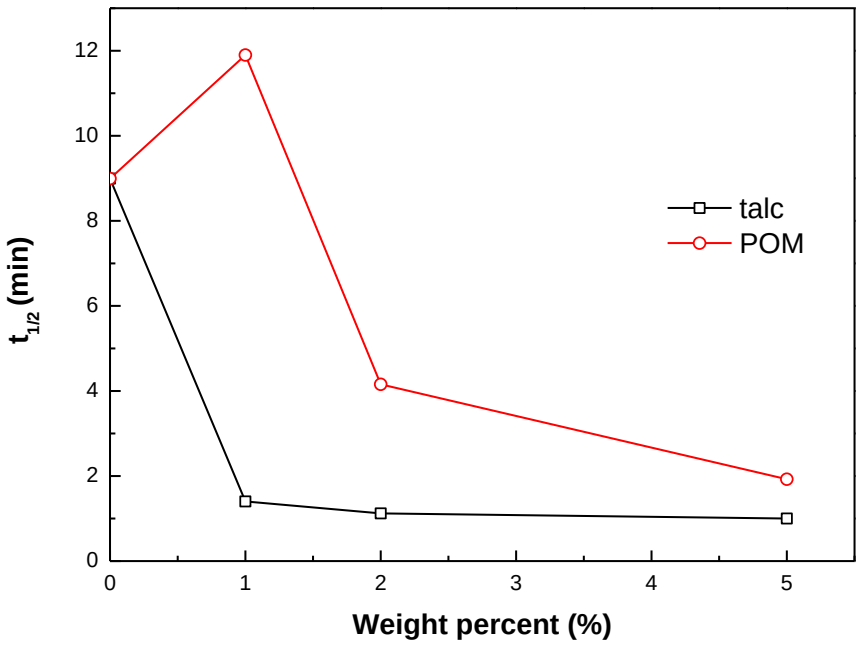

Figure 2.10. Curve of the half-time of crystallization versus different weight fractions of POM and talc respectively in the PLA/POM blends and PLA/talc blends

Another important parameter is the half-time of crystallization ($t_{1/2}$), which is introduced to directly compare the crystallization rate. $t_{1/2}$ is defined as the time from the onset of the crystallization until 50% completion and can be determined from the kinetics parameters.

$$t_{\frac{1}{2}} = \left(\frac{\ln 2}{K}\right)^{\frac{1}{n}} \qquad 2.4$$

The dependency of $t_{1/2}$ on the weight percent at 108 ^{o}C is shown in Figure 2.10. As seen in both POM and talc blends, the half-time of crystallization decreased with increasing the weight percent of the additives. Except for POM1 which shows a greater value of $t_{1/2}$ than that of neat PLA, dramatic decreases of $t_{1/2}$ were observed with the presence of POM (2 and 5 wt %) and talc (1, 2 and 5 wt %) when compared

to neat PLA, indicating the addition of POM and talc significantly enhanced the crystallization rate of PLA. Moreover, talc exhibited a higher effect than POM on improving the crystallization rate of neat PLA.

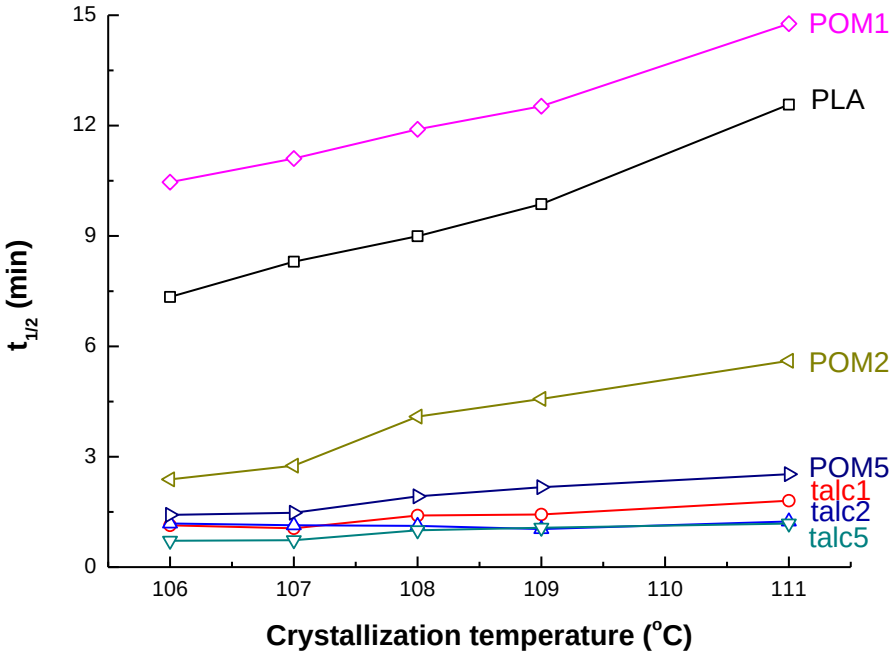

Figure 2.11. Curve of the half-time of crystallization versus different crystallization temperatures of neat PLA and its two blends with POM and talc

The plots of $t_{1/2}$ versus the crystallization temperature for neat PLA and its blends with POM and talc are showed in Figure 2.11. For each sample, the $t_{1/2}$ increases with crystallization temperature, indicating that the crystallization rate was faster when the degree of supercooling was greater. Moreover, values of $t_{1/2}$ for the PLA/talc blends were much smaller than those for the PLA/POM blends. Possible reasons are as follows: When the fine talc powder was uniformly dispersed in the PLA matrix, it would increase the number of sites for heterogeneous nucleation of PLA spherulites.

Therefore, the nucleation density in PLA/talc was significantly larger than that in PLA/POM, which made talc more effective than POM on enhancing the crystallization rate of PLA.

2.3.1.2 Nonisothermal crystallization of the PLA/POM blends

In practical processing, such as extrusion, injection molding and film production, crystallization usually proceeds under a nonisothermal process, so it is of practical significance to study the crystallization kinetics under nonisothermal conditions.

The nonisothermal crystallization of the PLA blends within 5 wt% POM were studied at different cooling rate ranging from 5 to 40°C/min. The crystallization exotherms shifted to lower temperatures with increasing cooling rate. This phenomenon is typical for nonisothermal crystallization of semicrystalline polymers. When the polymer crystallized at a lower cooling rate, the crystallization time is relatively longer within the temperature range that promoted sufficient mobility of segments for the growth of crystallites; when cooled at a higher rate, segments are frozen before the formation of crystallites, thereby decreasing the crystallization temperature.

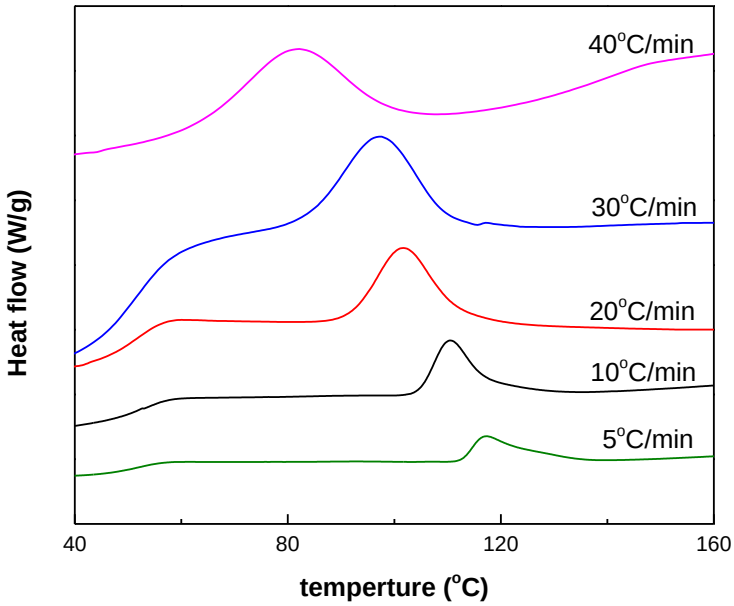

Figure 2.12. Thermograms of melt crystallization of PLA/POM=95/5 at different cooling rates.

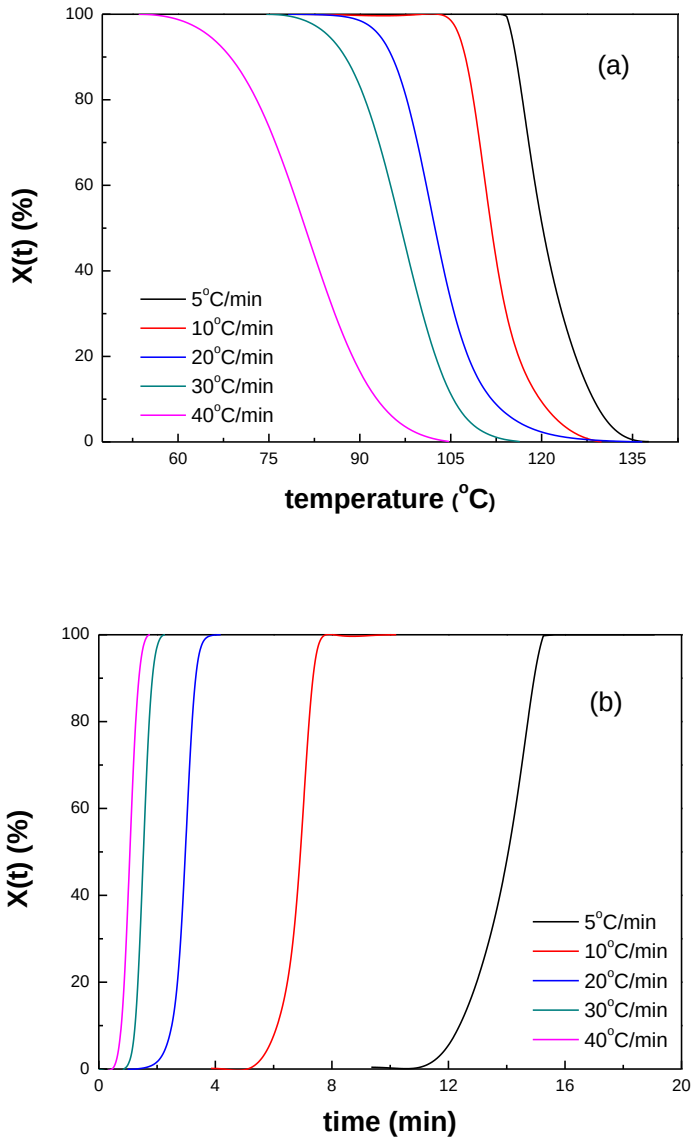

Figure 2.13. Curves of relative crystallization versus (a) crystallization temperature and (b) time for nonisothermal crystallization of PLA/POM=95/5

The relative crystallinity X(t) developing with crystallization time as shown in Figure 2.13(a) can be calculated from the DSC data. During the nonisothermal crystallization process, the curves display reversed S-shape. The horizontal temperature axis in Figure 2.13(a) can be transformed into a timescale in Figure

2.13(b) through equation 2.5 as follows:

$$t = \frac{|T_0 - T_c|}{R} \qquad 2.5$$

where T_0 is the initial temperature when crystallization begins (t=0) and R is the cooling rate. As shown in Figure 2.13(b), the higher cooling rate resulted in shorter crystallization time.

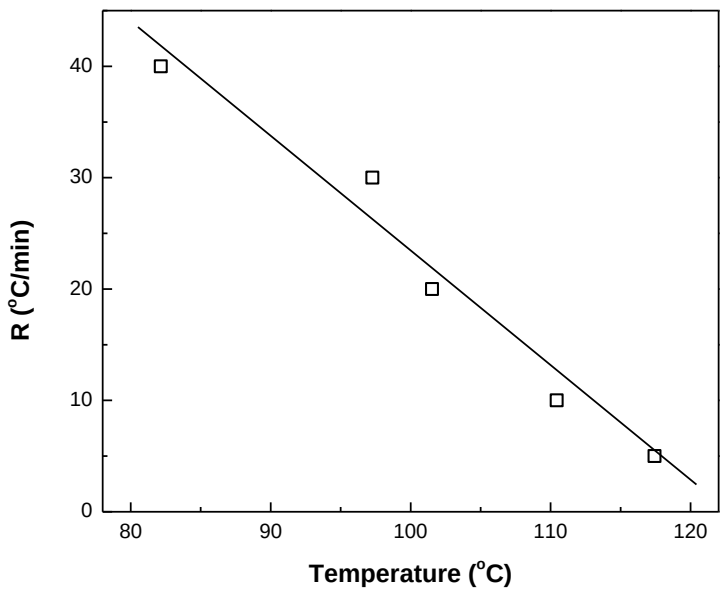

Figure 2.14. Dependency of the melt-crystallization peak temperature on the cooling rate (R) for nonisothermal crystallization of PLA/POM=95/5

To compare the crystallization rates of various polymers on a single scale, several empirical methods were proposed. Among them, Khanna et al. (1990) introduced a "crystallization rate coefficient" (CRC) defined as the variation in cooling rate required for a 1 ^{o}C-change in the undercooling of the polymer melt. The CRC can be measured from the slope of the plot of cooling rate versus crystallization peak temperature and can be used as a guide for ranking the polymers on a scale of

crystallization rates. Higher CRC values represent faster crystallization systems.

Based on Khanna's method, the cooling rate R is plotted against T in Figure 2.14. The CRC value of POM5 measured from the slope of the line is 62.76 h^{-1}, and the CRC value reported for neat PLA is 6.79 h^{-1} (Liu et al., 2005). Comparing the CRC values of POM5 and neat PLA, we can conclude that the CRC value of POM5 is much greater than neat PLA, which means the incorporation of POM enhance the crystallization of PLA and is beneficial for injection-molded fabrication resulting from the reduction in cycle time.

2.3.3 Crystallization morphology and crystalline growth of neat PLA and PLA blends

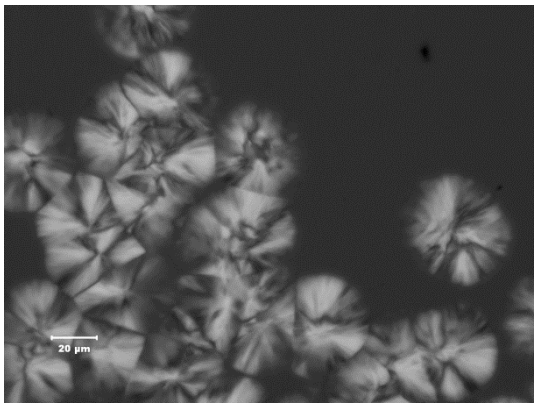

(a) neat PLA

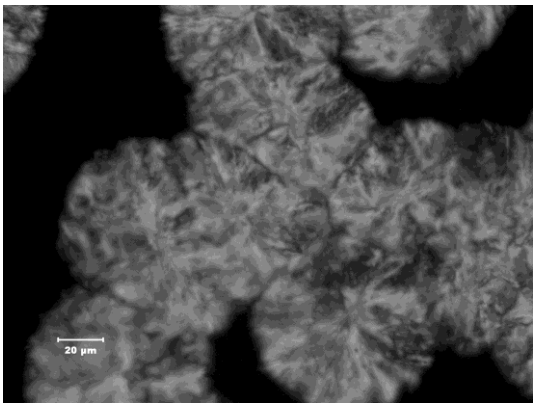

(b) neat POM

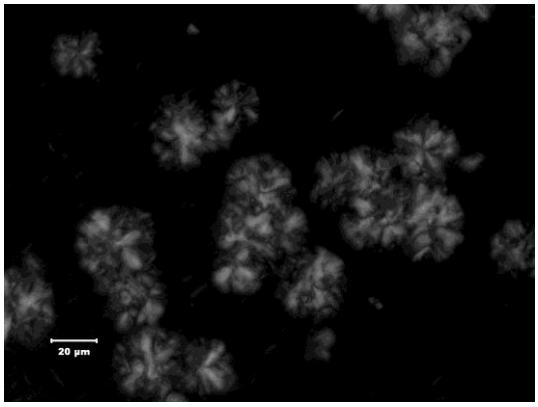

(c) POM1

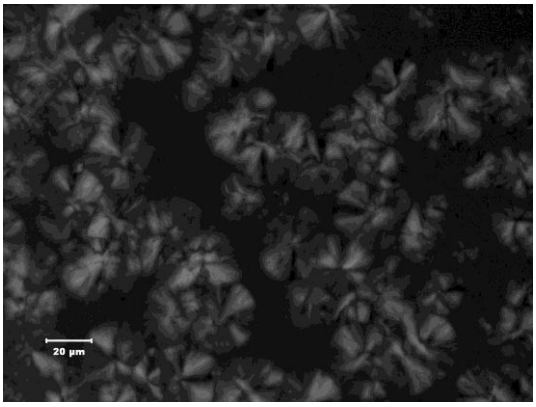

(d) talc1

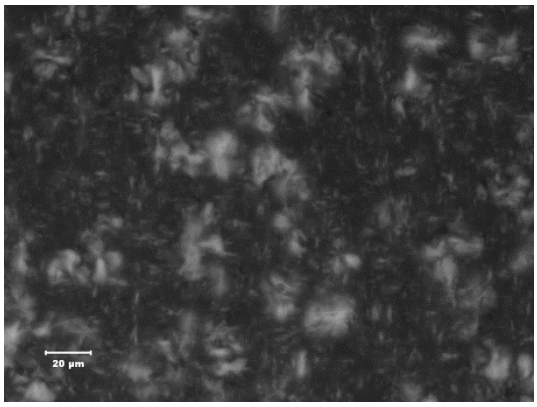

(e) POM2

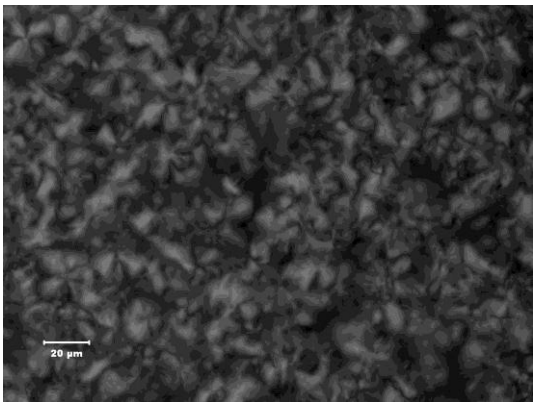

(f) talc2

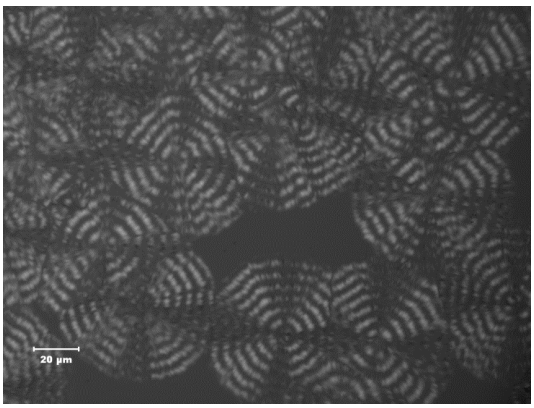

(g) POM5

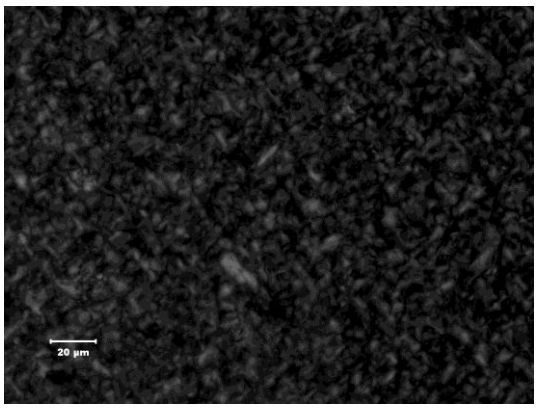

(h) talc5

Figure 2.15. Polarized optical micrographs of neat PLA, neat POM, PLA/POM blends and PLA/talc blends isothermally crystallized at 130 ^{o}C

For biodegradable crystalline polymers, the crystalline morphology and size are of importance in determining the physical and mechanical properties. Thus, the effects of nucleating agents in terms of type and concentration on the crystal morphology and spherulitic growth of PLA were studied using polarized optical microscopy. Figure 2.15 illustrates the spherulitic morphology of neat PLA, PLA blends and neat POM at 130 ^{o}C. As expected, a typical spherulitic morphology was observed for neat PLA in Figure 2.15a. In comparison with neat PLA, the PLA/talc blends had smaller spherulitic dimension and greater grain density as shown in the Figure 2.15 (d, f, h). Moreover, the crystal morphology of the PLA/talc blends were dependent on the loading level of talc in PLA. While the spherulitic dimension of the PLA/talc blends decreased with increased loading of talc, the grain density of the PLA/talc blends increased. In the case of PLA/talc blends, talc acted as a nucleating agent for the crystallization of PLA. This increased the number of crystal nuclei and caused the spherulites to impinge each other due to more crystal nuclei and space confinement, resulting in smaller dimension and denser distribution. By comparing Figure 2.15a and Figure 2.15b, the spherulitic dimension of neat POM is clearly larger than that of neat PLA. Nevertheless, Figure 2.15(c, e) illustrates that low loading levels (1 and 2 wt %) of POM in PLA did not increase the spherulitic dimension of PLA. When the loading of POM was 5 wt%, a well-defined banded spherulite was observed in Figure 2.15g. Compared to the PLA/POM blends, the PLA/talc blends had smaller spherulitic dimension and more densely populated spherulites which indicates that talc had more effective nucleation ability on the crystallization of PLA than POM.

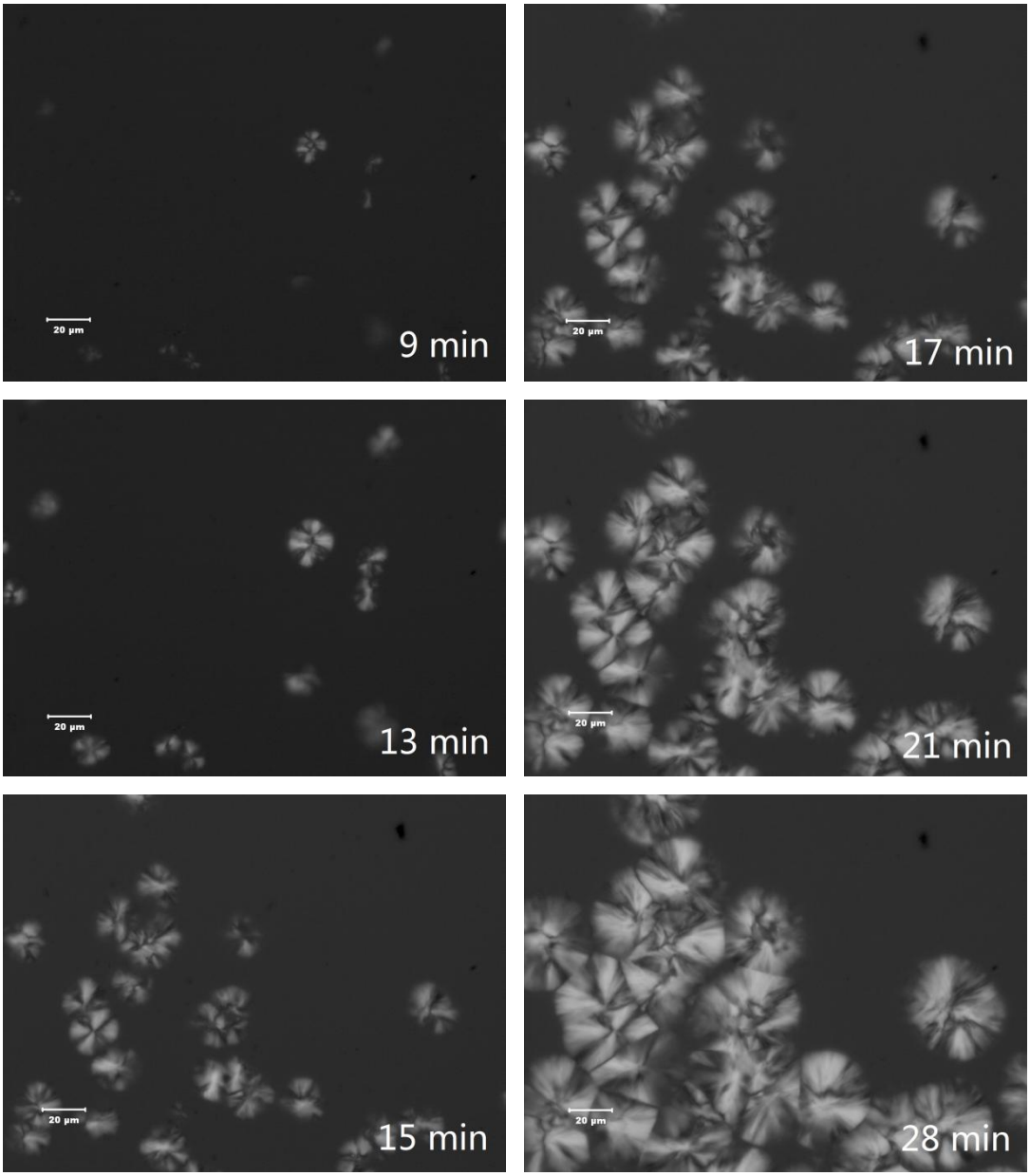

Figure 2.16. Crystalline growth of neat PLA during isothermal crystallization at 130 oC, the corresponding crystallization time is given in the graphs

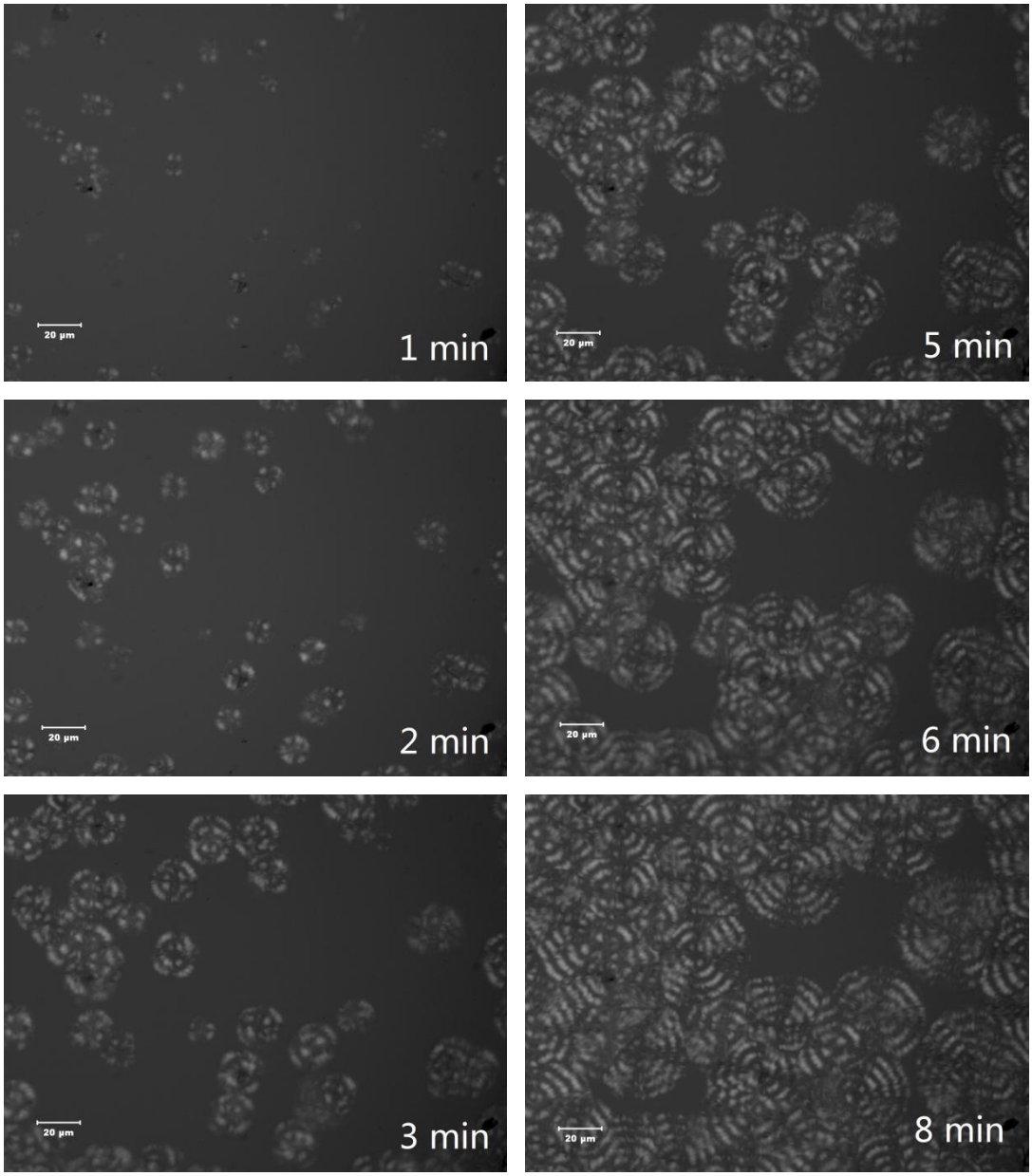

Figure 2.17. Crystalline growth of PLA/POM blends (PLA/POM=95/5) during isothermal crystallization at 130 oC, the corresponding crystallization time is given in the graphs

To reveal the subsequent crystal growth of neat PLA and its blends with 5 wt% POM, an in-situ polarized optical microscopy measurement was used. Figure 2.16 and Figure 2.17 show the evolution of spherulite structure for neat PLA and PLA/POM

blends, respectively, during isothermal crystallization at 130 ^{o}C. As shown in Figure 2.16, clear birefringence was not detected at the initial stage of crystallization (before 9 min) of neat PLA. Small Maltese cross spherulites were observed as crystallization time reached 13 min, while the spherulite distribution was sparse. With further increasing crystallization time, more spherulites were observed and the radius of the spherulite became larger and impinged on each other. Compared to the crystal growth process of neat PLA, POM5 had a faster crystallization rate since the birefringence arose at 1 min during isothermal crystallization at 130 ^{o}C, as illustrated in Figure 2.17. In 8 min, the well-defined banded spherulite was completely formed, the number of the spherulites and the radius of the spherulite increased with increasing crystallization time. It is clear from Figure 2.16 and Figure 2.17 that the 5 wt% POM significantly increased the crystallization rate of PLA and greatly changed the crystallization morphology of PLA from a typical spherulite with periodic extinction to a well-defined banded spherulite.

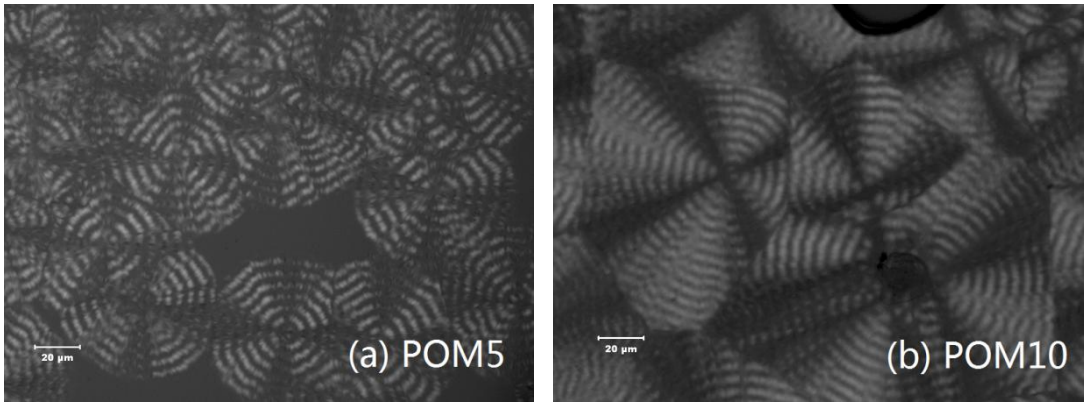

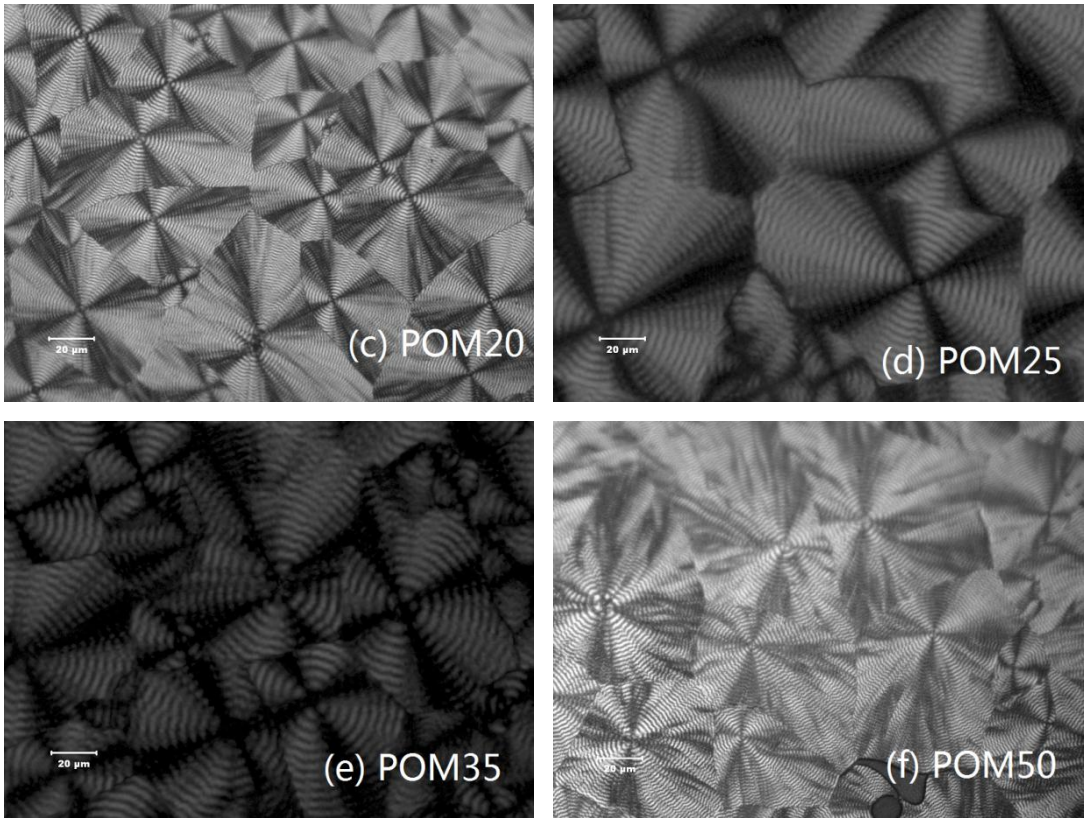

Figure 2.18. Polarized optical micrographs of the PLA/POM blends with various POM content: (a) 5; (b) 10; (c) 20; (d) 25; (e) 35; (f) 50 wt%.

Figure 2.18 shows the crystalline morphology of the PLA/POM blends with various weight fraction of POM. All samples were isothermally crystallized at 130 ^{o}C. The well-defined banded spherulites with characteristic Maltese cross extinction patterns were observed regardless of POM content. The Maltese cross is known to arise from a specific array of birefringent spherulites. Negative birefringence results from spherulites in which radial lamella are dominant, while positive birefringence is due to spherulites with predominantly tangential lamellae. Negatively and positively birefringent spherulites are alternatively arranged to form the Maltese cross under

crossed polarizers. It is generally believed that the banded spherulites result from the periodically lamellar twisting along the direction of radial growth, although this twisting is not usually uniform but changes of orientation take place discontinuously at periodic intervals (Chao et al., 2008). When such spherulites are viewed under crossed polarizers, the cross-section of the indicatrix perpendicular to the direction of propagation of the light through the spherulites periodically becomes circular and the polarization is unmodified as the light traverses the spherulites, so that dark circles appear at regular intervals in the addition to the Maltese cross to form the well-defined banded spherulits of PLA/POM blends.

2.3.4 Optical transparency of neat PLA and its blends

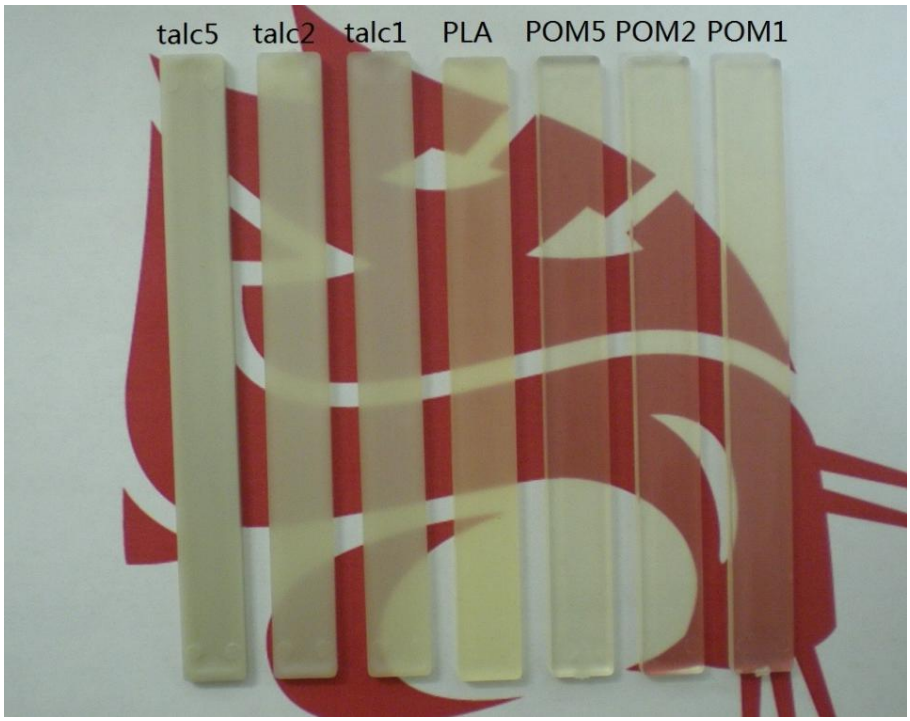

Figure 2.19. Photographs of neat PLA and PLA blends with POM and talc on a background paper for demonstrating their transparency

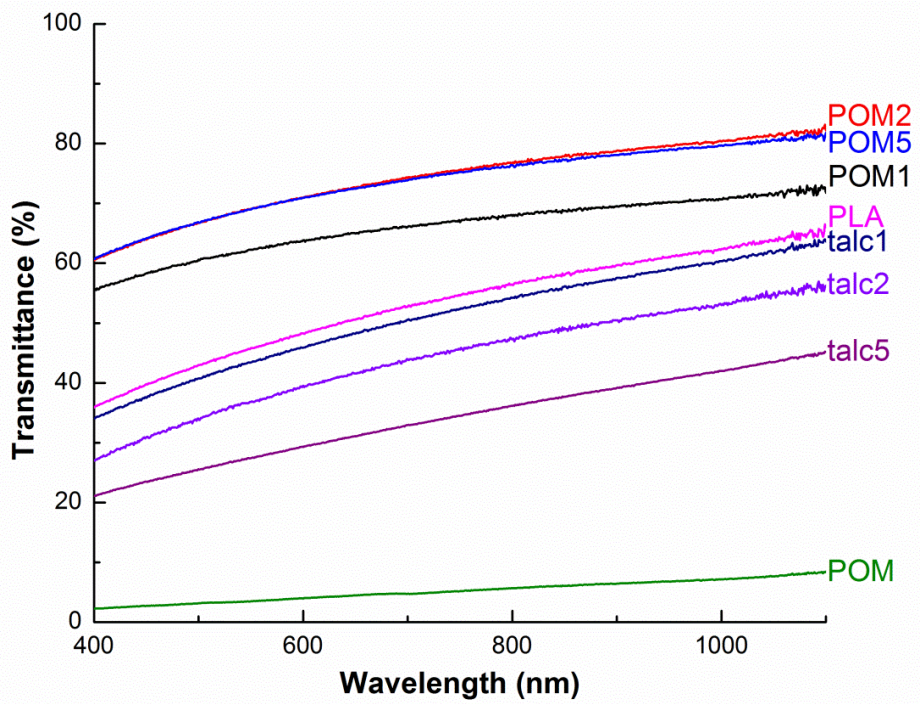

Figure 2.20. UV-vis transmittance spectra of neat PLA, neat POM, PLA/POM blends and PLA/talc bends

Figure 2.19 shows the comparison of transparency of neat PLA and PLA blends with POM and talc. Neat PLA appears translucent as the pattern and color is obscure behind the neat PLA specimen. In contrast, the pattern and color can be seen more clearly through the PLA/POM samples, suggesting that the blends at low POM loading levels exhibited higher transparency than neat PLA. However, the PLA/talc blends became more opaque.

The UV-vis transmittance spectra of neat POM, neat PLA and PLA blends with POM and talc at visible wavelength range (400-800 nm) are shown in Figure 2.20. All samples have a thickness of about 100 μm. The transmittance of PLA was significantly improved by the presence of POM , while the incorporation of talc

decreased the transmittance of PLA. Moreover, neat POM exhibited a very low transmittance (no greater than 10 %).

The high transparency of the PLA/POM may be attributed to the very similar refractive indices of PLA (1.482-1.492) (Rafael et al., 2010) and POM (1.476-1.492) (O'shea et al., 1992). Because the light scattering will not occur at the interface between the matrix and the filler if the refractive indices of the two components are identical, then transparent blends can result (Kutz et al., 2011). The transmittance of the blend is an effective way to judge the miscibility: immiscible blends are usually cloudy or opalescent because of the different refractive indices of the components. The fact that the incorporation of POM did not decrease, instead, increased the transmittance of PLA, indicating PLA/POM blends are miscible or semi-miscible. The transmittance of the PLA/talc blends was lower than that of neat PLA and decreased with the increase in talc loading because of the heterogeneous nature of the blends. Usually, for a transparent polymer, modification of the matrix by dispersing an inorganic component into the polymer results in a significant loss of transparency due to scattering from large particles or agglomerates (Dusek et al., 2010). Another possible reason for the reduction of the transmittance is the increase of crystallinity of PLA by the presence of talc, since the crystals in the blends scatter light (Philip et al., 2002).

2.3.5 Crystal structure of PLA blends

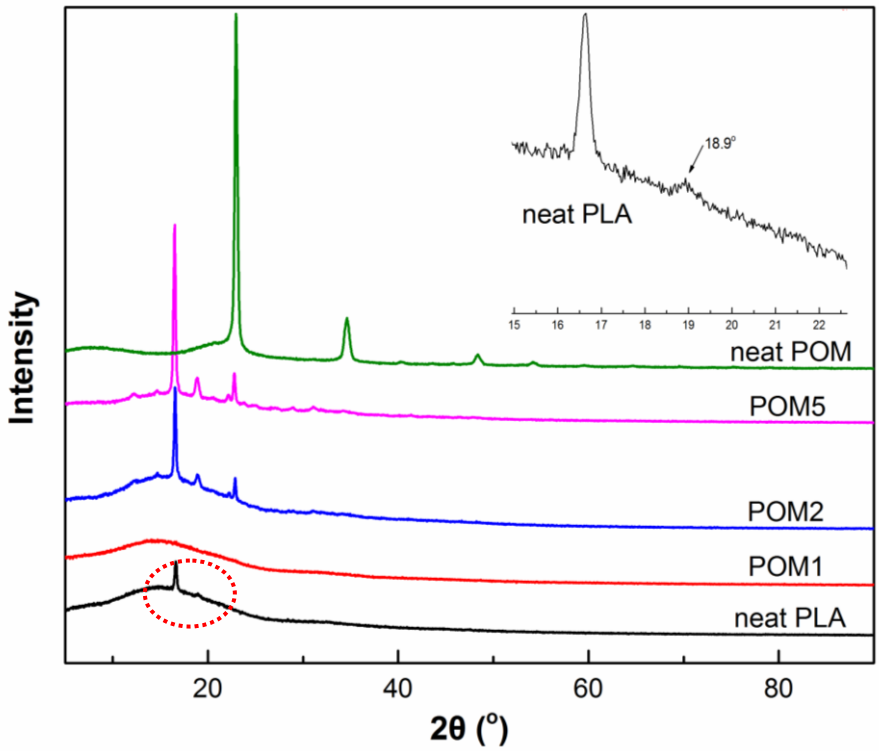

Figure 2.21. XRD patterns of neat POM, neat PLA and the PLA/POM blends, all film samples were isothermally hold at 120 ℃ for 45 min.

To get further information of crystallization of neat PLA and its blends, the crystalline nature of neat PLA and its blends was analyzed by X-ray diffraction. Figure 2.21 shows the XRD patterns of neat PLA and its blends with POM annealed at 120 ^{o}C for 45 min from the melt. Neat PLA presents two main diffraction peaks at 16.6 and 18.9^{o} which respectively correspond to the (110/200) and (203) plane of α-form orthorhombic crystal lattice (Shi et al., 2012; Nakajima et al., 2010; Tsuji et al., 2011). Neat POM demonstrates two main diffraction peaks at around 23 and 34.6^{o} ascribed to the (100) plane of hexagonal crystal lattice of POM (Wang et al., 2008; Li et al., 2007). Compared to neat PLA, POM1 presented a smooth curve without any diffraction peaks, while POM2 and POM5 showed a characteristic diffraction peak of

POM at around 22.8^{o} in addition to those featured diffraction peaks of PLA at 16.6 and 18.9^{o}. Therefore, the presence of POM didn't change the crystal structure of PLA because the characteristic peaks of PLA and POM respectively maintained in PLA/POM blends without forming any new peak. Moreover the peak intensities of the PLA/POM blends increased with increase of POM content, indicating that the presence of POM increased the crystallinity of PLA except when the loading level of POM was 1 wt% or lower, as low content of POM (less than 1 wt)% impeded the crystallization of PLA. The result of XRD corresponded to the DSC results of crystallization and crystalline morphology, and suggests that the proper content of POM in PLA can enhance the crystallization of POM.

It is of significance to study the influence of different fillers on the crystal structure of PLA. Figure 2.22 illustrates the XRD patterns of neat PLA and its blends with POM and talc quenched from the melt. Neat PLA and POM1 exhibited smooth curves with a bump around 16°. POM2 and POM5 presented a weak characteristic diffraction peak of POM at 22.8 due to the (100) plane of hexagonal crystals. The PLA/talc blends exhibited three strong diffraction peaks at around 9.5, 18.9 and 28.6^{o} corresponding to the (002), (020) and (006) panes of talc (Kano et al., 1998; Ferrage et al., 2002). The PLA/talc blends have sharper peaks and higher values of intensity when compared with the PLA/POM blends. The result suggests that talc is more effective than POM on enhancing the crystallization of PLA, which is consistent with the conclusion of the crystallization kinetics measured by DSC.

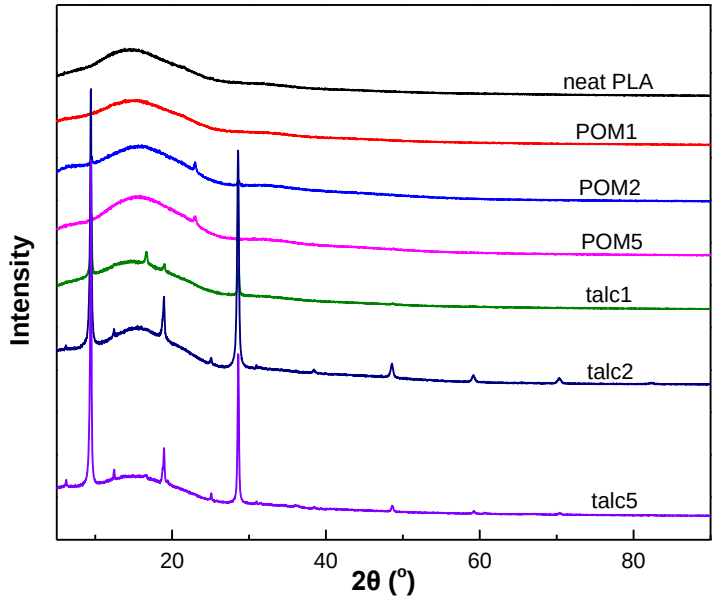

Figure 2.22. XRD patterns of neat PLA and its two blends with POM and talc, all film samples were quenched from the melt

2.3.6 Miscibility of the PLA/POM blends

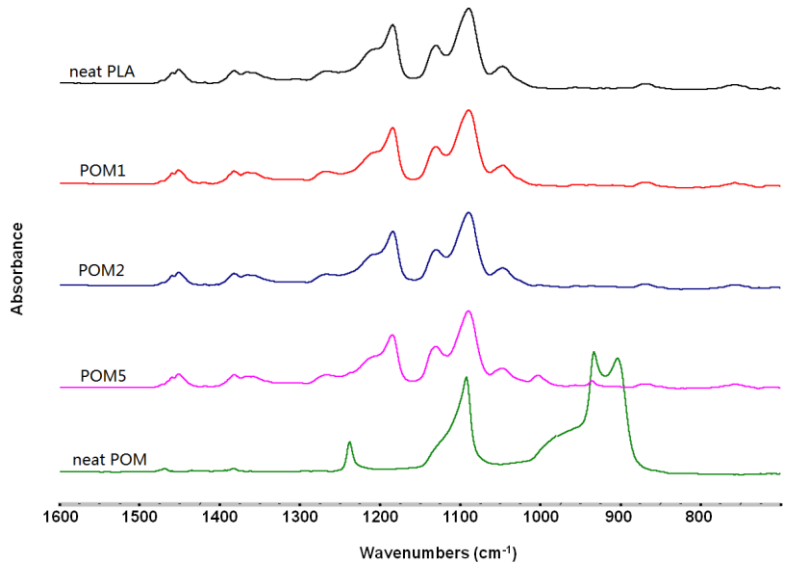

Figure 2.23. FTIR spectra in the wavenumber range of 700-1600 cm^{-1} of neat POM, neat PLA and PLA/POM blends

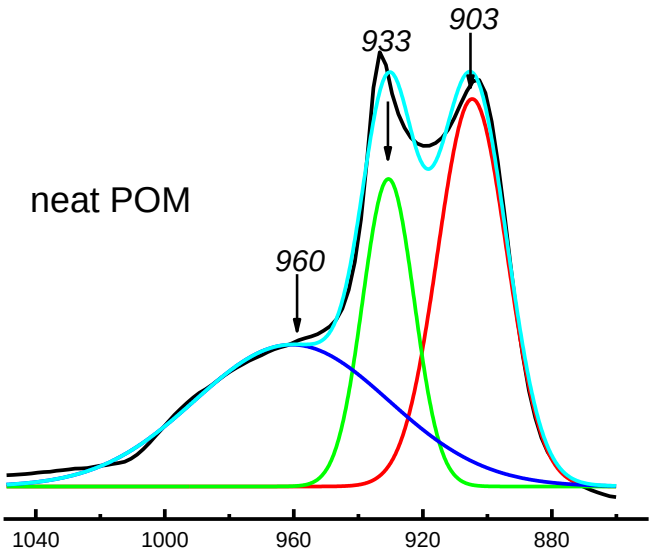

Figure 2.24. Deconvolution curve of neat POM in the wavenumber range 900-1050 cm-1

FTIR spectroscopy was used to detect the miscibility of POM and PLA. The enlarged spectra ranged from 700 to 1600 cm^{-1} as plotted in Figure 2.23. A strong absorbance band at 1755 cm^{-1}, attributed to the stretching vibrations of carbonyl group (C=O) (Buzarovska et al 2012), is shown in spectra of neat PLA and its blends with POM, but not in neat POM. The strong absorption bands located at 1089 and 1184 cm^{-1} are due to the C-O-C stretching vibrations for neat PLA and its blends with POM (Wu et al 2007). For neat POM, the major absorption bands at 903, 933, 1092 and 1238 cm^{-1} are due to the symmetric and asymmetric stretching vibrations of C-O-C ether groups (Ramirez et al., 2011; Chang et al., 1991). Figure 2.24 showed the deconvolution of the hump around 980 cm^{-1} in neat POM. The hump splitted into the characteristic peak at 960 cm^{-1}. The medium absorption bands positioned in the

range of 1300-1500 cm^{-1} for all samples are owed to symmetric and asymmetric deformational vibrations of C-H in CH_3 groups (Pamula et al., 2001). It is clear that the spectra of POM1 and POM2 are identical with neat PLA, no characteristic peaks of POM at 903, 933 and 1238 cm^{-1} are detected in the spectra. However, two characteristic absorption bands are observed for POM5 at 935 and 1001 cm^{-1} when compared to neat PLA. The band at 935 cm^{-1} is shifted to the right when compared with the neat POM at 933 cm^{-1}, also due to the C-O-C stretching vibration. The characteristic absorption band at 1001 cm-1 is neither originated from PLA nor POM, indicating an obvious chemical interaction between PLA and POM. Therefore, the PLA/POM blends are considered miscible or partially miscible. This is consistent with the result of transmittance obtained by UV-vis.

2.3.7 Morphology of cryo-fractured surfaces of neat PLA and PLA blends

The phase structures of the binary blends were examined using SEM. Figure 2.25 shows the cryo-fractured surface SEM micrographs of neat PLA and various PLA blends. Neat PLA presents a relatively smoother surface than the PLA/POM blends, as terraces with irregular shape and clear edges appeared on the surfaces of the PLA/POM blends. Except for that, there is no difference between the neat PLA and the PLA /POM blends. The small particles and holes were found for both neat PLA and the PLA/POM blends. Therefore, the PLA/POM blends presented single-phase structure indicating PLA and POM is miscible or semi-miscible, which was in agreement with the transmittance and FTIR results.

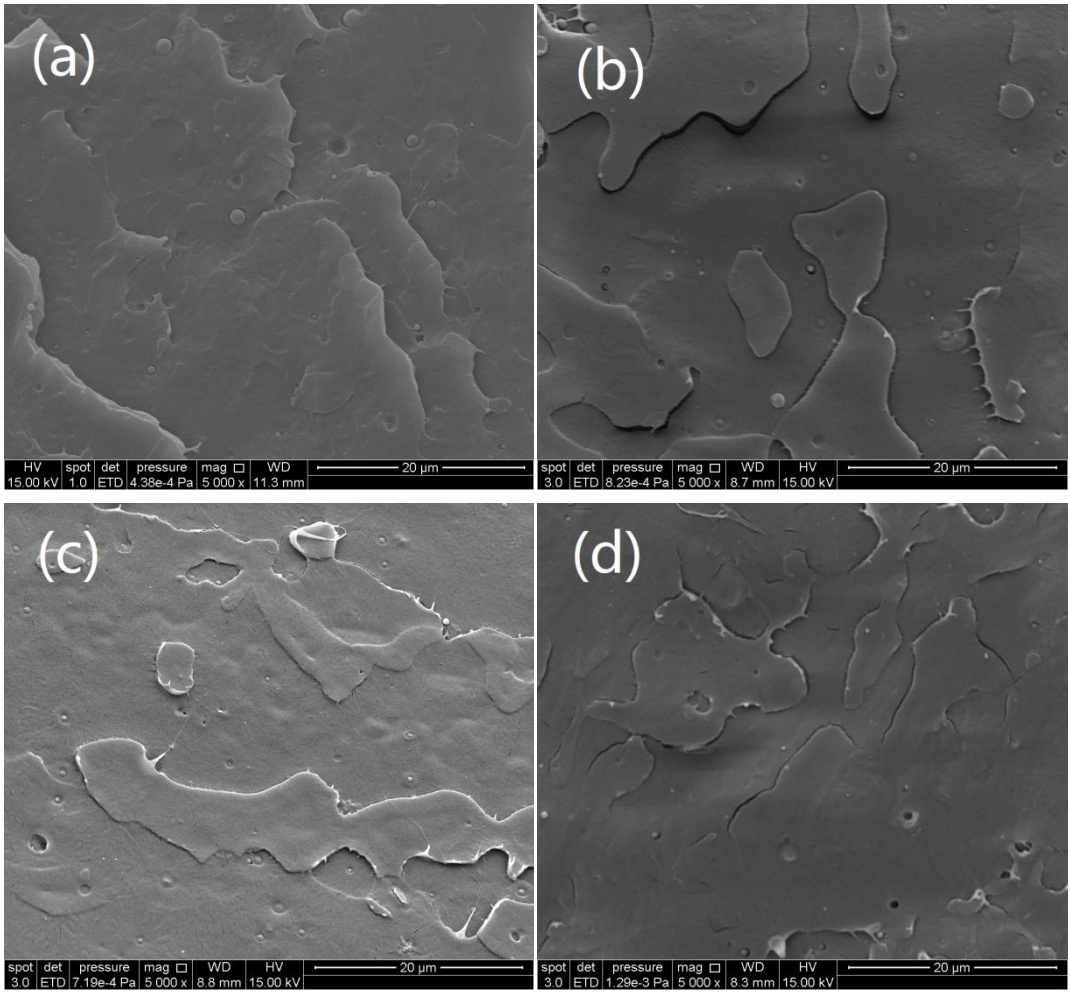

Figure 2.25. Cryo-fractured SEM images of blends: (a) neat PLA, (b) POM1, (c) POM2 and (d) POM5

2.3.8 Mechanical properties of neat PLA and its blends

Tensile properties of neat PLA and PLA blends with POM and talc are given in Table 2.5. Tensile properties of neat PLA were not dramatically changed by the presence of POM and talc, which was probably due to their low loading level, while the PLA/talc blends presented a higher modulus than neat PLA, and the PLA/POM blends maintained similar modulus as neat PLA. Addition of 5 wt% of POM to PLA

resulted in an increase in impact strength increased 12.7 J/m of neat PLA to 19.6 J/m for the blend, while addition of same amount of talc only increased the impact strength to 15.2 J/m. Moreover, impact strength increased with filler content.

Table 2.5. Mechanical Properties of neat PLA and its two blends with POM and talc

Sample		Modulus	Tensile strength	Elongation at break	Impact strength
		GPa	MPa	%	J/m
neat PLA		3.36±0.06	62.1±0.65	3.9±0.5	12.7±0.02
neat POM		2.74±0.04	57.6±0.3	31.6±6.95	30±3.03
PLA/POM blends	99/1	3.38±0.04	64.2±0.43	4.7±0.35	13.6±0.06
	98/2	3.37±0.06	62.8±0.64	4.6±0.27	13.6±0.3
	95/5	3.32±0.07	59±0.41	4.5±0.44	19.6±2.33
PLA/talc blends	99/1	3.64±0.03	62.9±0.73	3.8±0.7	12.7±0.06
	98/2	3.78±0.02	62.9±0.69	4±0.53	14.4±0.7
	95/5	4.56±0.05	61.2±0.5	3.5±0.31	15.2±1.87

2.4 Conclusions

Both greater enthalpy and lower cold crystallization temperature of PLA/POM blends during DSC the first heating exhibited improvement in crystallization ability of PLA by the addition of POM. During isothermal crystallization, the crystallization

rate of PLA was improved by the presence of POM and talc. Moreover, talc is more effective than POM in improving the crystallization rate of PLA. Well-defined banded spherulites were observed for PLA/POM blends when the POM content was greater than 5 wt%. PLA/POM blends exhibited higher transparency than both PLA and PLA/talc blends indicating PLA/POM blends might be partially miscible. XRD results displayed that PLA/POM blends reserved the characteristic peaks of PLA and POM without forming any new peak, exhibiting the crystal structure of PLA was not changed by the presence of POM. The distinct characteristic peaks at 1001 cm^{-1} of PLA/POM blends in FTIR spectra indicated obvious chemical interactions between PLA and POM, exhibiting PLA/POM blends were partially miscible consistent with the transparency results. PLA/POM blends presented smooth and homogenous surfaces. Besides modulus of PLA were increased by the presence of both POM and talc.

Reference

Kawamoto, N.; Sakai, A.; Horikohi, T., "Nucleating agent for poly(L-lactic acid)-An optimization of chemical structure of hydrazide compound for advanced nucleation ability." Journal of Applied Polymer Science, (2007) 103 (1): 198-203.

Defosse, M., Modern Plastics, January 1, 2005.

Kawamoto, N.; Tobita, E.; Goman, P., Polyolefins 2003; Society of Plastics Engineers: Houston, TX, 2003.

Funamizu, T.; Goman, P.; Kawamoto, N.' Polyolefins 2005; Society of Plastics Engineers: Houston, TX, 2005.

Nakajima, H.; Takahashi, M.; Kimura Y., "Induced Crystallization of PLLA in the Presence of 1,3,5-Benzenetricarboxylamide Derivatives as Nucleators: Preparation of Haze-Free Crystalline PLLA Materials." Macromol. Mater. Eng., (2010) 295: 460-468.

Maiti, P.; Nam, P. H.; Okamoto, M., "Crystallization on Intercalation, Morphology, and Mechanical Properties of Polypropylene/Clay Nanocomposites." Macromolecules, (2002) 35: 2042-2049.

Gagnon, K. D.; Lenz, R. W.; Farris, R. J.; Fuller, R. C., "Crystallization behavior and its influence on the mechanical properties of a thermoplastic elastomer produced by Pseudomonas oleovorans." Macromolecules (1992) 25: 3723-3728.

Tang, Z.; Zhang, C.; Liu, X., "The Crystallization Behavior and mechanical Properties of Polylactic Acid in the Presence of Crystal Nucleating Agent." Journal of Applied Polymer Science, (2011).

Shi, Q. F.; Mou, H. Y.; Li, Q. Y., "Influence of Heat Treatment on the Heat Distortion Temperature of Poly(lactic acid)/Bamboo Fiber/Talc Hybrid Biocomposites." Journal of Applied Polymer Science, (2012) 123: 2828-2836.

Garlotta, D., "A Literature Review of Poly(Lactic Acid)." Journal of Polymers and the Environment, (2001) 9: 63-84.

Barrau, S.; Vanmansart, C.; Moreau, M., "Crystalliztion Behavior of Carbon Nanotube-Polylactide Nanocomposites." Macromolecules, (2011) 44: 6496-6502.

Wunderlich, B., Macromolecular Physics; Academic Press: New York, 1977; Vol. 2.

Liu, T.; Mo, Z.; Wang, S., "Nonisothermal melt and cold crystallization kinetics of

poly(aryl ether ether ketone ketone).” Polymer Engineering & Science, (1997) 37 (3): 568-575

Dell’Erba, R.; Groeninckx, G.; Maglio, G., “Immiscible polymer blends of semicrystalline biocompatible components: thermal properties and phase morphology analysis of PLLA/PCL blends.” Polymer, (2001) 42: 7831-7840

Khanna, Y., “A barometer of crystallization rates of polymeric materials.” Polymer Engineering & Science, (1990) 30 (24): 1615-1619.

Liu, T.; Lin, W.; Yang, M., “Miscibility, thermal characterization and crystallization of poly(L-lactide) and poly(tetramethylene adipate-co-terephthalate) blend membranes.” Polymer, (2005) 46: 12586-12594.

Rafael, A., Poly(lactic acid): synthesis, structure, properties, processing, and Application; Loong-Tak, Lim; Wiley, 2010: 508

O’shea, S.; Swettenhan, K.; Revell, P. “A sipme optical method for the differentiation of two types of polymeric wear debris in tissue samples.” Journal of Material Science: Materials in Medicine (1992) 3 (6): 391-396.

Kutz, M., Applied Plastics Engineering Handbook: Processing and Materials. Elsevier. 2011: 463

Dusek, K., Polymer Characterization: Rheology, Laser Interferometry, Electrooptics. Springer. 2010: 280

Philip, M., Technology of Engineering Materials. Elsevier. 2002: 471

Buzarovska, A.; Grozdanov, A., “Biodegradable Poly(L-lactic acid)/TiO2 Nanocomposites: Thermal Properties and Degradation.” Journal of Applied Polymer Science, (2012) 123: 2187-2193.

Wu, D.; Wu, L.; Wu, L., “Nonisothermal Cold crystallization Behavior and Kinetics of Polylactide/Clay Nanocomposites.” Journal of Polymer Science: Part B: Physics, (2007) 45: 1100-1113.

Ramirez, N. V.; Sanchez-Soto, M.; Illescas, S., “Enhancement of POM Thermooxidation Resistance Through POSS Nanoparticles.” Polymer Composites, 2011: 1584-1592.

Chang, F.; Yang, M.; Wu, J., “Blends of Polycarbonate and Polyacetal.” Polymer, (1991) 32 (8): 1394-1400.

Pamula, E.; Blazewicz, M.; Paluszkiewicz, C.; Dobrzynski, P., “FTIR study of degradation products of aliphatic polyesters-carbon fibers composites.” Journal of Molecular Structure, (2001) 596: 69-75.

Tsuji, H.; Tashiro, K.; Bouapao, L., “Synchronous and separate homo-crystallization of enantiomeric poly(L-lactic acid)/poly(D-lactic acid) blends.” (2011) 53: 747-754.

Wang, J.; Hu, K. H.; Xu Y. F., “Structural, Thermal, and Tribological Properties of Intercalated Polyoxymethylene/Molybdenum Disulfied Nanocomposites.” Journal of Applied Polymer Science, (2008) 110: 91-96.

Li, K.; Xiang, D.; Lei, X., “Green and Self-Lubricating Polyoxymethylene Composites Filled with Low-Density Polyethylene and Rice Husk Flour.” Journal of Applied Polymer Science, (2008) 108: 2778-2786.

Kano, J.; Saito, F., “Correlation of Powder characteristics of talc during Planetary Ball Milling with the impact energy of the balls stimulated by the Particle Element Method.” Powder Technology, (1998) 98: 166-170.

Ferrage, E.; Martin, F., “Talc as nucleating agent of polypropylene morphology induced by lamellar particles addition and interface mineral-matrix modelization.” Journal of Materials Science, (2002) 37: 1561-1573.

Chapter 3 Properties and structure of PLA/POM blends with excellent heat resistance

Abstract

The thermodynamic properties and phase morphology were examined using dynamic mechanical analysis (DMA), differential scanning calorimetry (DSC) and the scanning electron microscopy (SEM). Heat deflection temperature (HDT) of poly(lactic acid) (PLA) was improved by incorporating polyoxymethylene (POM), a highly crystalline polymer with excellent heat resistance. The HDT of neat PLA was increased nearly 2-fold from 65.5 ^{o}C to 133 ^{o}C by adding 50 wt% POM. Fourier transform infrared spectroscopy (FTIR) and the Fox equation was used to identify the miscibility of the PLA/POM blends and found that the PLA/POM blends are partially miscible. The toughening effect of two type of elastomers based on the PLA/POM blend (50/50), viz, thermoplastic polyurethane (TPU) and poly(ethylene-glycidyl methacrylate) (EGMA) were investigated in detail in this study. The experimental results suggested that TPU was more effective in toughening the PLA/POM blend than EGMA.

Keyword: heat deflection temperature, miscibility, toughening, mechanical properties

3.1 Introduction

Poly(lactic acid) is a biodegradable polymer derived from renewable resources. The biodegradability and biocompatibility envisions PLA as a promising alternative to traditional petroleum-based polymers. Despites many advantages of PLA such as high tensile strength and modulus, the inherent brittleness (poor impact strength and elongation at break) and the low HDT extremely limit the application of PLA as engineering plastics. Several papers have reported that the blends of PLA with poly(ε-caprolactone) (PCL), poly(butylene adipate-co-terephthalate) (PBAT), poly(butylenes succinate) (PBS) and poly(hydroxyl butyrate) (PHB) improve the toughness and elongation of PLA (Nanda et al., 2011; Broz et al., 2003; Semba et al., 2006; and Zhang et al., 2009). The impact strength is improved to a degree but is still not enough for PLA to be used as engineering plastics.

HDT of PLA is very low and is known to be around *Tg* (60 ^{o}C), because the crystallinity is very low under practical molding conditions due to the low crystallization rate of PLA at a high cooling rate (Baiardo et al., 2003; Tsuji et al., 1995; Jiang et al., 2007; and Liu et al., 2011). Currently, two primary methods are used to improve the HDT of PLA. The first method is to obtain a stereocomplex by adding PDLA homopolymer into PLLA (Brizzolara et al., 1996). The stereocomplex is 1:1 complex of PDLA and PLLA. The improvement of HDT is ascribed to the higher crystallinity of the stereocomplex than those of PLLA and PDLA. However, the stereocomplex requires long cycle time to form, and PDLA is not commercially

available at a viable cost. The second method is to increase the crystallinity by adding a nucleating agent into PLA. The addition of an appropriate nucleating agent to the semicrystalline polymer increases the crystallization rate and maintains even increases the mechanical properties as well (Angela et al., 2008). In this research, POM is chosen to blend with PLA to increase the HDT of PLA. There have been no studies which blend PLA with POM and study the effects of POM on HDT yet. The primary reason for choosing POM is that POM presents very high HDT at about 160 ^{o}C at 0.46 MPa. In addition, the melting temperature of POM (175 ^{o}C) is close to that of PLA, which makes it easier to blends PLA with POM through melting extrusion.

3.2 Experimental

3.2.1 Materials

All the materials used in this study are listed in Table 3.1

Table 3.1. Characteristics of materials in this study

Materials (abbreviation)	Grade (supplier)	Specifications
Poly(lactic acid) (PLA)	PLA 2002D (NatureWorks)	MI(201 ^{o}C, 2.16kg) = 5~7g/10min Specific Gravity = 1.24
Polyoxymethylene (POM)	RTP 800 (RTP Co.)	Specific Gravity = 1.41
Thermoplastic Polyurethane (TPU)	Elastollan C95A10 (BASF Co.)	Specific Gravity = 1.21
Poly(ethylene-glycidyl methacrylate) (EGMA)	IGETABOND^{TM} (Sumitomo Chemical Co.)	MI (190 ^{o}C, 2.16kg) = 12 g/10 min Specific Gravity = 0.94

All materials in this study were used as received without further purification.

3.2.2 Preparation of the PLA/POM blends

Prior to extrusion, all pellets were dried at least 1 day at 85 ^{o}C in a convection oven to remove moisture in the samples. PLA and the fillers were premixed manually through tumbling in a sealed plastic bag. A co-rotating twin-screw extruder (Leistritz ZSE-18) equipped with a volumetric feeder and a pelletizer was used to prepare the

PLA/POM blends. The screw diameter and L/D ratio of the extruder were 17.8 mm and 40, respectively. The screw speed was maintained at 50 rpm for all runs, and the temperature profile of the barrel was (160, 160, 200, 200, 200, 170, 150 and 150 ^{o}C) from the first heating zone (next to the feeding throat) to die. The extrudate was cooled under water and subsequently granulated by the pelletizer. The ratio of the two polymer components (PLA/POM) in the blends were 75/25, 65/35, 60/40 and 50/50 (w/w), respectively. Neat PLA and POM were prepared under the same conditions and used as controls. TPU and EBA-GMA were added in the PLA/POM blends (PLA/POM = 50/50) to toughen PLA, the weight fractions are 5 % and 10 % for TPU, and 2 %, 5%, 10 % and 20 % for EBA-GMA (based on 100 parts of the blends). Before injection molding, the blends were dried at 85 ^{o}C for 1 day in a convection oven. Standard tensile (ASTM D638, Type I) test specimens were prepared using injection molding (Sumitomo SE 50D) at melt temperature of 190 ^{o}C and a mold temperature of 40 ^{o}C. After injection molding, all specimens were conditioned at 23 ^{o}C and 50% RH for 7 days prior to characterization.

3.2.3 Characterization

Dynamic mechanical analysis (DMA). Dynamic mechanical properties of the PLA/POM blends and their components (neat PLA and neat POM) were studied with DMA Q800 (TA Instruments) in a single-cantilever mode with an oscillating frequency of 1 Hz. DMA specimens with dimensions of about $13\times3\times35$ mm^3 were cut from injection molded samples. All tests were conducted using a 3 ^{o}C/min with

temperature ramp from -50 ^{o}C to 150 ^{o}C. To detect the glass transition temperature and heat deflection temperature of POM, the temperature was scanned from -100 ^{o}C to 175 ^{o}C.

Differential scanning calorimetry (DSC). Crystallization behavior of the blends was studied by differential scanning calorimeter (Mettler Toledo, DSC 822e). The sample sizes were about 5 mg, and were crimp sealed in 40-μL aluminum pans, each sample was tested in duplicates. To determine the crystallization and melting temperatures, the samples were first heated up to 200 ^{o}C at 10 ^{o}C/min and held isothermally for 5 min to erase the thermal history, then cooled to 0 ^{o}C at 10 ^{o}C/min, and finally heated up to 200 ^{o}C at the same rate.

Heat deflection temperature (HDT). The HDT for the samples were estimated from plots of log E ´versus temperature using a technique developed by Scobbo (Paul et al., 2000); the HDT is defined by ASTM standards (ASTM E2092) as the temperature at which the center deflection of a standard specimen in a three point bend mode reaches 0.25 mm under an applied maximum stress of 0.46 MPa. The HDT at a stress of 0.46 MPa corresponds to the temperature at which the logarithm of storage modulus, log E ´is 8.3.

Scanning electron microscopy (SEM). Cryo-fractured surfaces of neat PLA and PLA blends samples were examined using a Quanta 200F field emission scanning

electron microscope (FE-SEM, FEI Co.) at an accelerated voltage of 15 kV. All specimens were sputter-coated with gold prior to examination.

Fourier Transform Infrared Spectroscopy (FT-IR). The absorption spectra were recorded using a Thermo Nicolet Nexus 670 spectrometer (Nicolet, Thermo Scientific) with a resolution of 4 cm^{-1} and 32 scans and a Smart iTR (Thermo Scientific) with a pointed pressure tip and a crystal plate of Ge crystal. The sheets of neat PLA and its blends with POM used for characterization were prepared by melting and then quickly quenched to room temperature.

Mechanical test. Tensile tests were conducted on a universal testing machine (Instron 4466) following ASTM D638 (type I specimens). The crosshead speed was 0.2 in/min (5.08 mm/min) for all the specimens, and the initial strain was measured using a 2 in (50.8 mm) extensometer. Notched Izod impact tests were performed according to ASTM D256 using a BPI-0-1 Basic Pendulum Impact tester (Dynisco, MA). Average value of five replicates was taken for each formulation.

3.3 Results and discussion

3.3.1 Thermodynamic properties of the PLA/POM blends

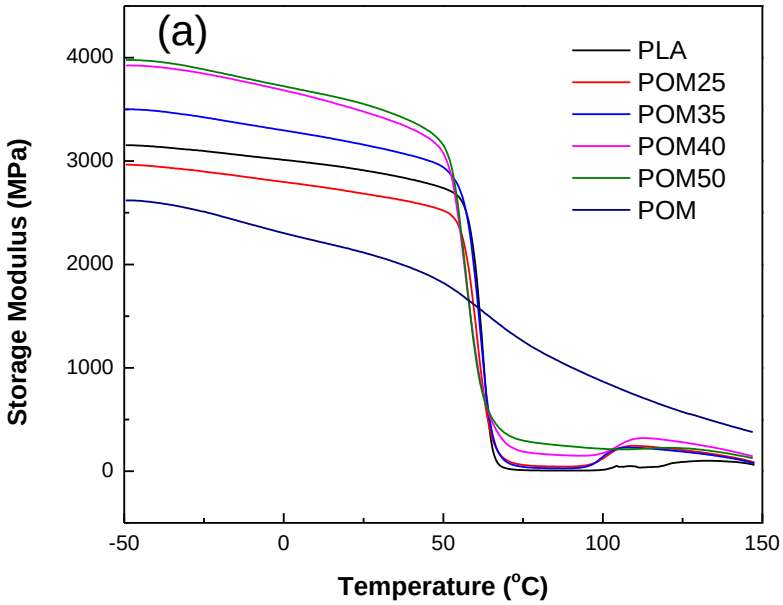

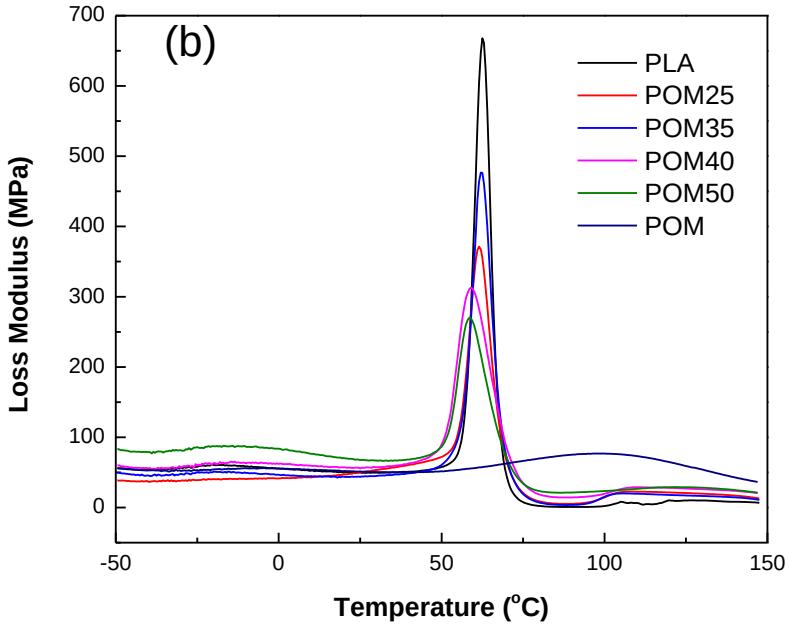

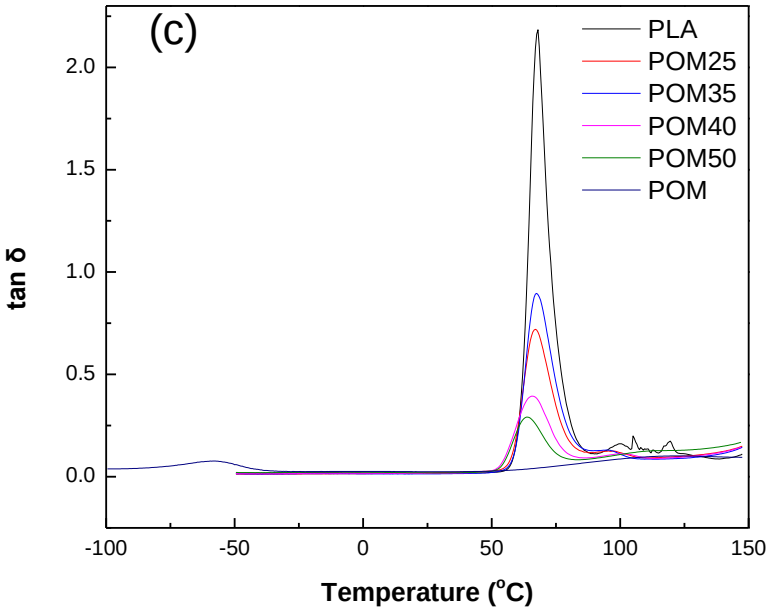

Figure 3.1. Dynamic mechanical properties of the PLA/POM blends: (a) storage modulus, (b) loss modulus and (c) tan δ.

Dynamic mechanical properties of the PLA/POM blends and neat components were investigated by DMA. The blends with 25, 35, 40 and 50 wt% of POM are hereafter denoted as POM25, POM35, POM40 and POM50, respectively. Below the T_g of PLA, PLA and its blends with POM exhibited much higher storage modulus (E ´) than POM whose storage modulus decreased across the whole temperature range. The storage modulus of the PLA/POM blends except for POM25 below T_g was higher than that of neat PLA. For example, the E ´at 25 ^{o}C increased from 2.91 GPa for neat PLA to 3.48 and 3.55 GPa for POM40 and POM50, respectively. Compared with neat PLA, POM40 and POM50 displayed increase of 19.5% and 22%, respectively. This improvement in E ´ at temperature below T_g may be attributed to the increased

crystallinity of PLA blends by the presence of POM, indicating that POM can enhance the stiffness of PLA. At the glass transition, E' of PLA and the PLA/POM blends precipitated sharply around 60 ^{o}C. The loss moduli of neat PLA and the PLA/POM blends increase around 60 ^{o}C, as shown in Figure 3.1(b), and this is in agreement with the storage modulus data. An increase of E´was noted around 110 ^{o}C for neat PLA and the PLA/POM blends, which was due to the PLA cold crystallization. The increase in E´induced by the cold crystallization is more distinct and occurs at relatively low temperature in the PLA/POM blends because the presence of POM increase the crystallization rate of PLA.

Figure 3.1(c) shows the loss factors (tan δ) of the PLA/POM blends and the pure components as a function of temperature, where the ratio of loss modulus to storage modulus gives the tangent of the phase angle delta, a measure of energy dissipation. The tan δ peak position corresponding to the T_g and the peak height values are presented in Table 3.2. T_g of the blends gradually decreased as the POM content in the blends increased, ranging from T_g = 68 ^{o}C of neat PLA to T_g = 63.5 ^{o}C for PLA in POM50. This result suggests POM was partially dissolved in the PLA phase, leading to the depression of T_g. The Fox equation can be used to estimate the partial miscibility (Fox et al., 1956).

$$\frac{1}{T_{gb'}} = \frac{W_1'}{T_{g1}} + \frac{(1 - W_1')}{T_{g2}} \qquad 3.1$$

Here, T_{g1} and T_{g2} are the T_gs of neat PLA and POM, respectively, and the $T_{gb'}$ is the T_g of POM50; $(1-w_{1'})$ is the weight fraction of POM in the PLA/POM blends. Introducing the values into Equation 3.1, an estimate of about 2.3 wt% of POM dissolved in the PLA phase is obtained.

The height of the peak represents the relative energy dissipated over the stored energy per cycle. The values of tan δ in the PLA/POM blends decrease in height with increasing POM content. The decrease of the damping value with higher amounts of the nonviscous is a well-known effect observed in semicrystalline polymers (Sarasua et al 1998). Thus, this behavior could be attributed to the enhanced crystallinity of PLA in presence of POM.

Table 3.2. Glass transition temperature of the PLA/POM blends and its components (neat PLA and neat POM)

Sample	T_g (^oC)	tan δ
neat PLA	68	2.18
POM25	67	0.72
POM35	67.5	0.89
POM40	66	0.39
POM50	63.5	0.29
neat POM	-58.5	n.a.

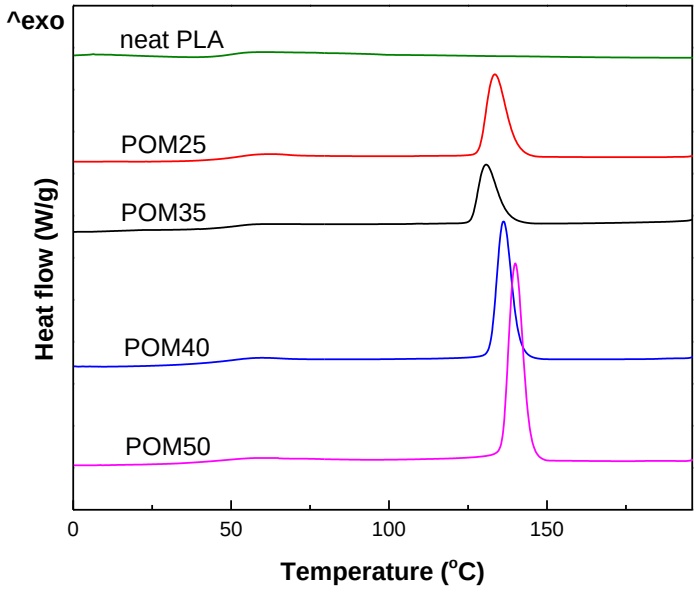

Figure 3.2. First cooling DSC curves of the PLA/POM blends

Table 3.3. DSC parameters of cooling and crystallinity for the PLA/POM blends

Sample	$T_{m,c}$ (°C)	χ_c (%)
neat PLA	n.a.	n.a.
POM25	133.5	11.7
POM35	130.8	8.6
POM40	136	17.1
POM50	140	28

As shown in chapter 2, the crystallization rate of neat PLA is very slow and the half-time of crystallization is in the range of 7.3 – 12.6 min. POM is an effective nucleating agent in the process of PLA crystallization, the half-time of crystallization during isothermal crystallization at 111 ^{o}C was decreased nearly 5-fold by adding 5% POM. In this chapter, the effect of high POM content on the crystallization behavior of PLA was studied through DSC. Figure 3.2 shows the first cooling curves of the PLA/POM blends. The crystallinity (χ_c) was calculated according to the following equation:

$$\chi_c = \frac{\Delta H_m}{W_f \times \Delta H_m^{\infty}} \times 100\% \qquad 3.2$$

Where ΔH_m is the enthalpy of melting crystallization during cooling scan; ΔH_m^{∞} is the enthalpy assuming 100% crystalline PLA (93.7 J/g), and W_f is the weight fraction of PLA component in the blends. The DSC parameters are listed in Table 3.3.

As expected, POM greatly enhances the crystallization of PLA since obvious exotherms were observed during cooling process, while no exotherm was detected for neat PLA. Table 3.3 shows that the crystallinity increases with POM content, for example, the crystallinity of POM25 increased nearly 3-fold from 11.7% to 28% of POM50. The noticeable increase of cystallinity suggests that the high POM content steeply improves the crystallization ability of PLA.

3.3.2 Heat Deflection temperature of the PLA/POM blends

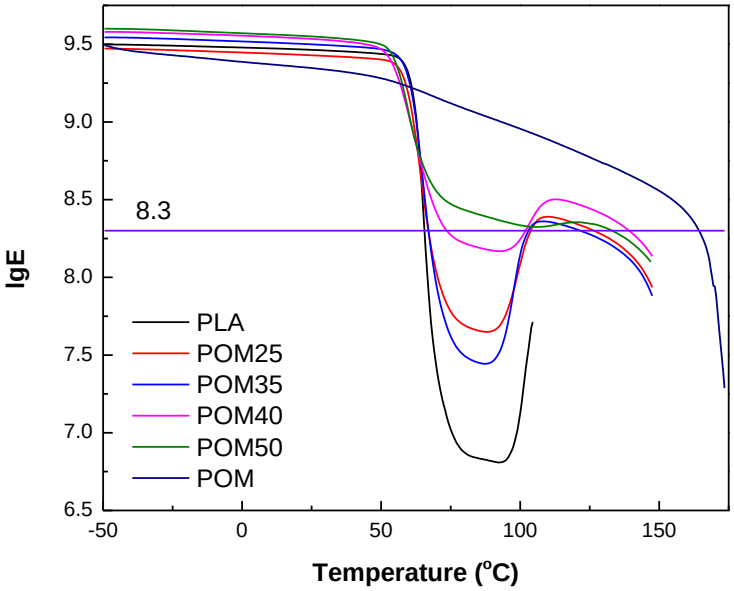

Figure 3.3. Dynamic mechanical properties of the PLA/POM lends

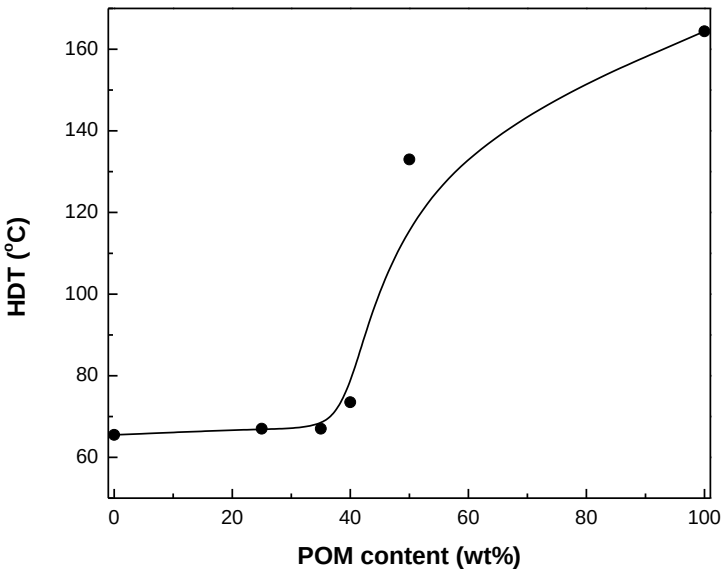

Figure 3.4. HDT of the PLA/POM blends

Table 3.4. HDT of PLA, POM and their blends

Sample	HDT (^{o}C) at 8.3
neat PLA	65.5
POM25	67
POM35	67
POM40	73.5
POM50	133
neat POM	164.4

The dynamic mechanical properties of samples were studied to indicate the influence of POM on heat deflection temperature (HDT) in the PLA blends, since HDT represents the ability of polymeric material to withstand loads at elevated temperature. The HDT values of polymer also could be estimated by DMA results (Paul et al 2000). The HDT of the PLA/POM blends at a stress of 0.46 MPa corresponds to the temperature when the logarithm of storage modulus (Pa; log E') is 8.3 and is plotted in Figure 3.3. The trend of HDT versus POM content was showed in Figure 3.4. As expected, the HDT of PLA/POM blends increases with POM content and is greater than that of neat PLA. The HDT was barely raised by adding 25 and 35 wt% POM and started to noticeably increase when the addition of POM larger than 40 wt%. The HDT values of the PLA/POM blends are listed in Table 3.4. The HDT of neat PLA and POM are 65.5 and 164.4 ^{o}C, respectively which corresponds to the

general believing that the HDT of an amorphous polymer is around its Tg and that of a highly crystalline polymer is at the vicinity of its melting point. The HDT of PLA was increased nearly 2-fold by adding 50 wt% POM from 65.5 ^{o}C to 133 ^{o}C. This improvement of HDT is mainly due to the increase of crystallinity of PLA. According to the results in DSC tests, neat PLA is amorphous while the PLA/POM blends are semicrystalline, and the crystallinity increases with increasing POM content. The crystallinity of POM50 is about 2-time greater than that of POM25, therefore the HDT of POM50 is much greater than that of POM25 whose HDT is similar to that of neat PLA.

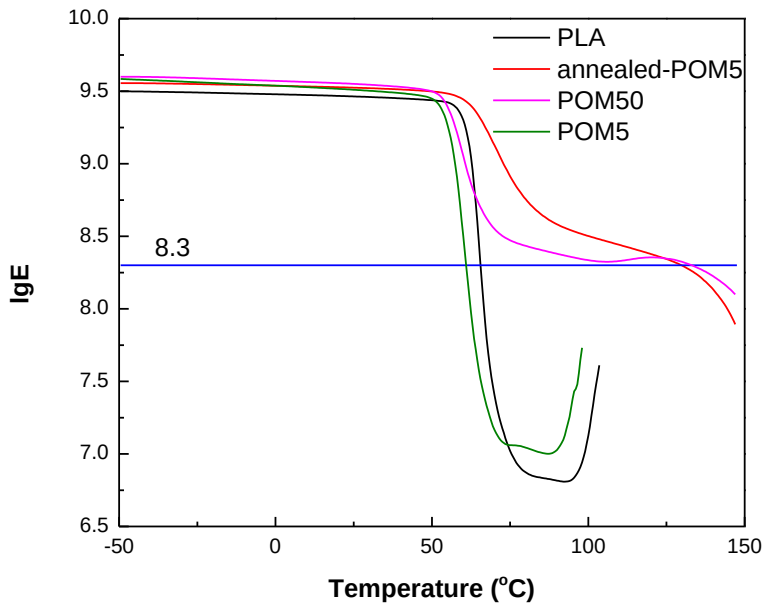

Figure 3.5. Dynamic mechanical properties of the PLA/POM lends with and without heat treatment

Table 3.5. HDT of the PLA/POM blends with and without heat treatment.

Sample	HDT (^{o}C) at 8.3
PLA	65.5
POM5	61
a-POM5	129.7
POM50	133

To realize the effect of heat treatment on the HDT of the PLA/POM blends, the POM5 sample was annealed at 85 ^{o}C for 45 min. The logarithm of storage modulus (Pa; log E') of the PLA/POM blends versus temperature is plotted in Figure 3.5, the HDT corresponds to the temperature when the logarithm of storage modulus is 8.3 (0.46 MPa). Figure 3.5 shows that the HDT of POM5 (without heat treatment) is lower than that of neat PLA, whereas the HDT of annealed POM5 is highly greater than that of neat PLA. The HDT values of neat PLA and the PLA/POM blends are summarized in Table 3.5. The HDT of neat PLA decreased from 65.5 to 61 ^{o}C by adding 5 wt% POM before annealing, however the HDT of POM5 increased from 61 to 129.7 ^{o}C after annealing, indicating the annealing process can greatly increase the HDT of PLA. The improvement of HDT is attributed to the increase of crystallinity since the annealing process provides a chance for the blends to further crystallize at elevated temperature and resulted in higher crystallinity of the blends. The HDT of annealed POM5 is 129.7 ^{o}C which is very similar to the HDT of untreated POM50

(133 ^{o}C), indicating the annealing process can steeply improve HDT of the PLA/POM blends at very low POM content (5 wt%) and obtain almost the same effect on increasing HDT of adding 50 wt% to POM w/o annealing.

3.3.3 Miscibility and morphology of the PLA/POM blends

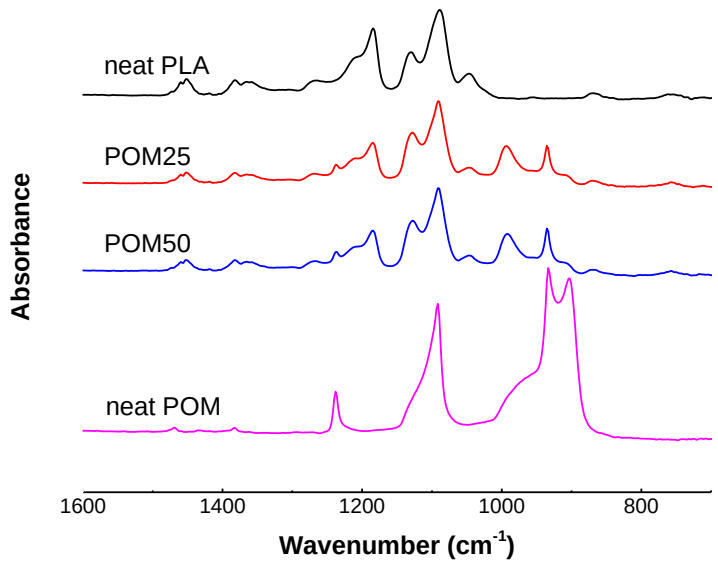

Figure 3.6. FTIR spectra in the wavenumber range of 700-1600 cm^{-1} of neat POM, neat PLA and PLA/POM blends.

FTIR spectroscopy was used to detect the miscibility of POM and PLA. Figure 3.6 presents the FTIR spectra of neat POM, neat PLA and its blends with POM. A strong absorbance band at 1755 cm^{-1}, attributed to the stretching vibrations of carbonyl group (C=O) (Buzarovska et al., 2012), is shown in spectra of neat PLA and

its blends with POM, but not in neat POM. The strong absorption bands located at 1089 and 1184 cm^{-1} are caused by the C-O-C stretching vibrations for neat PLA and its blends with POM (Wu et al., 2007). For neat POM, the major absorption bands at 903, 933, 1092 and 1238 cm^{-1} are due to the symmetric and asymmetric stretching vibrations of C-O-C ether groups (Ramirez et al., 2011; Chang et al., 1991). The medium absorption bands positioned in the range of 1300-1500 cm^{-1} for all samples are owed to symmetric and asymmetric deformational vibrations of C-H in CH_3 groups (Pamula et al., 2001). Two characteristic absorption bands are observed for POM25 and POM50 at 935 and 992 cm^{-1} when compared with neat PLA. The band at 935 cm^{-1} is slightly shifted to right compared with the neat POM at 933 cm^{-1}, also due to the C-O-C stretching vibration. The characteristic absorption band at 992 cm-1 is neither originated from PLA nor POM, indicating an obvious chemical interaction between PLA and POM. Therefore, the PLA/POM blends are considered to be partially miscible, which is consistent with the result of Fox equation.

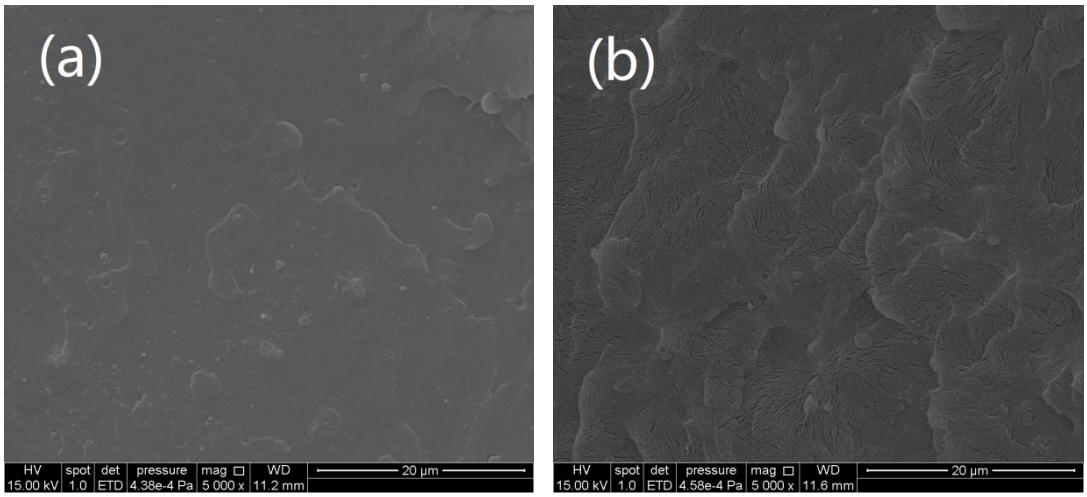

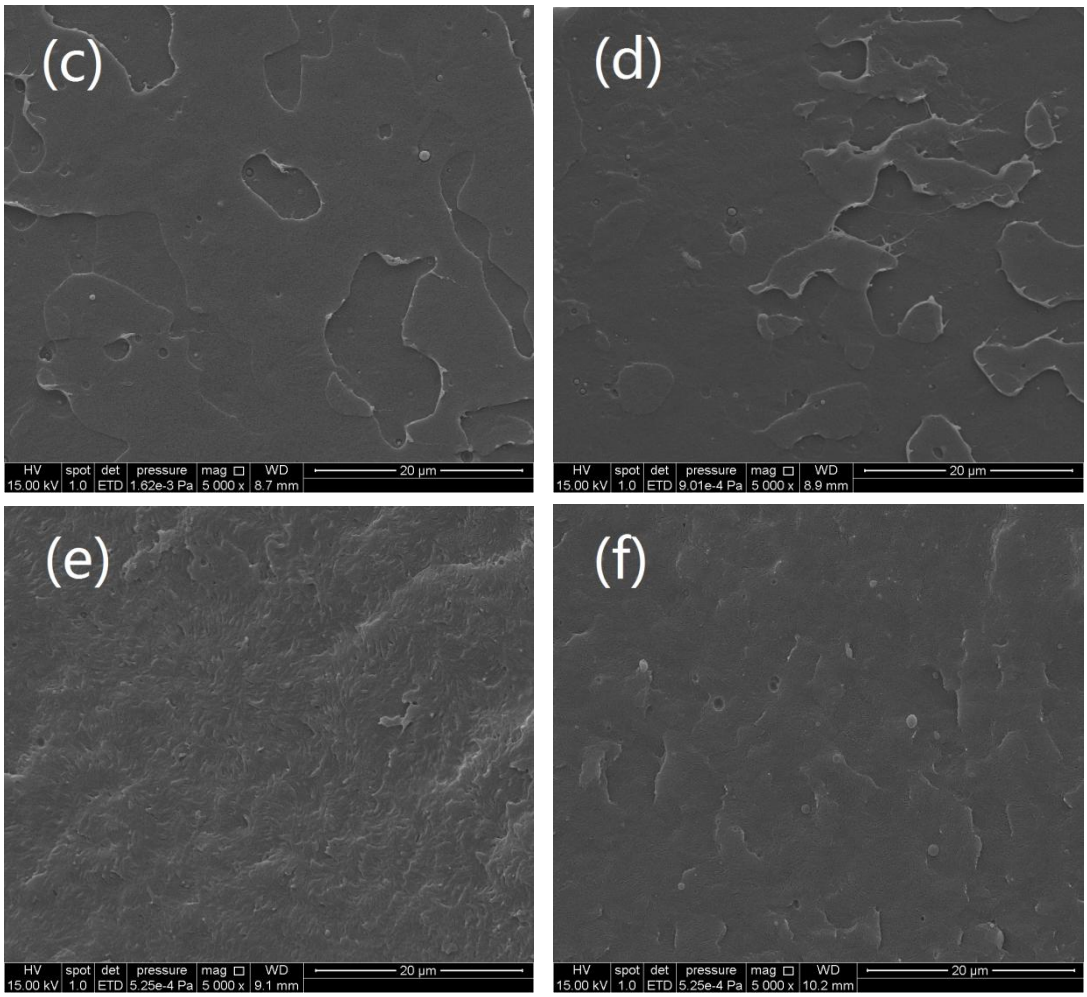

Figure 3.7. Cryo-fractured SEM images of the PLA/POM blends: (a) neat PLA, (b) neat POM, (c) POM5, (d) POM10, (e) POM25 and (f) POM50

The morphology structure of the PLA/POM blends was observed using SEM. Figure 3.7 shows the cryo-fractured surface SEM micrographs of PLA, POM and their blends. Compared with the relatively smooth surface of neat PLA, terraces with irregular shape and clear edges were observed on the surfaces of POM5 and POM10. There were many fine cracks/macroscopic phenomenon of spherulites disorderly arranged on the surface of the neat POM. The multiple-crack structure was not observed for neat PLA, POM5 and POM10 but detected in POM25 and POM50. The

multiple-crack structure of POM25 is more noticeable than that of POM50, and the fine cracks of POM25 agglomerated to form chrysanthemum-like structure. The characteristic structure of the PLA/POM blends containing 25 and 50 wt% POM could lead to the differences in thermodynamic and mechanical properties of PLA.

3.3.4 Mechanical properties of the PLA/POM blends

Table 3.6. Mechanical Properties of neat PLA, neat POM and their blends

Sample		Modulus	Tensile strength	Elongation at break	Impact strength
		GPa	MPa	%	J/m
neat PLA		3.36±0.06	62.1±0.65	3.9±0.5	12.7±0.02
neat POM		2.74±0.04	57.6±0.3	31.6±6.95	30±3.03
PLA/POM	75/25	3.57±0.07	60.5±0.85	2.9±0.71	16.1±0.72
	65/35	3.39±0.04	58.2±0.65	3.4±0.33	17.2±0.05
	60/40	3.78±0.06	57.5±0.37	3.3±0.31	16.5±0.48
	50/50	3.67±0.04	54.7±0.2	13.8±0.57	15.2±0.39

Tensile and impact properties of the PLA/POM blends are listed in Table 3.6. POM exhibited a much smaller modulus (2.74 GPa) than PLA (3.36 GPa). However, PLA/POM blends had higher moduli than both neat PLA and POM regardless of POM content. The increase in modulus of the PLA/POM blends was mainly ascribed

to the increase in crystallization of PLA by adding POM as a polymeric nucleating agent. Tensile strength of the PLA/POM blends decreased with increasing POM content. The elongation at break of neat POM was 10 times that of neat PLA, while the PLA blends containing 25, 35 and 40 wt% POM exhibited lower elongation at break compared to neat PLA. The elongation at break of the PLA blends with 50 wt% POM increased from 3.9% of neat PLA to 13.8%. The impact strength of the PLA/POM blends was slightly higher than that of neat PLA. As shown in Table 3.6, the impact strength is improved 36.5% from 12.69 J/m to 17.18 J/m by adding 35 wt% POM.

Table 3.7. Mechanical properties of neat PLA, POM50 and its two ternary blends

Sample		Modulus	Tensile strength	Elongation at break	Impact strength
		GPa	MPa	%	J/m
neat PLA		3.36±0.06	62.1±0.65	3.9±0.5	12.7±0.02
PLA/POM=50/50		2.74±0.04	57.6±0.3	31.6±6.95	30±3.03
PLA/POM/ TPU	47.5/47.5/5	3.3±0.03	48.3±0.67	5.9±0.32	42.6±1.21
	45/45/10	2.99±0.03	43.9±0.8	9.8±0.73	57±0.75
PLA/POM/ EGMA	49/49/2	3.63±0.06	55.7±0.31	14.4±0.48	23±0.64
	47.5/47.5/5	3.41±0.03	53.3±0.63	13.1±0.23	26.5±0.56
	45/45/10	3.08±0.04	49.4±0.45	13.9±0.17	32.3±0.81
	40/40/20	2.56±0.06	40.2±0.72	35.9±0.76	72.3±1.42

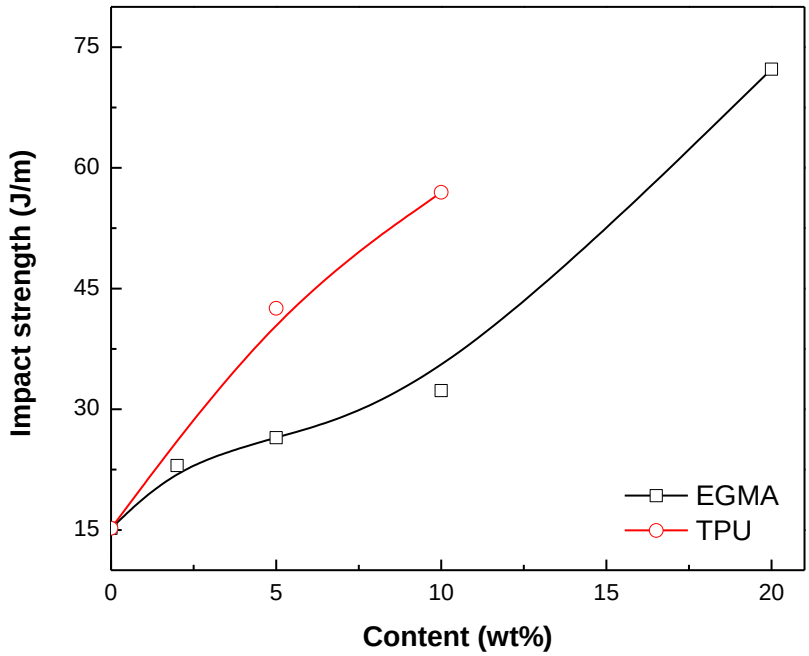

Figure 3.8. Impact strength of ternary blends versus elastomer content

To obtain good-toughened PLA blends with excellent heat resistance, thermoplastic polyurethane (TPU) and poly(ethylene-glycidyl methacrylate) (EGMA) were added to POM50, respectively. Comparing with POM50, the additions of TPU and EGMA as elastomers decrease the modulus and tensile strength. The modulus and tensile strength of the two ternary blends decreased when increasing the content of modifiers (TPU and EGMA). TPU is a biodegradable elastomer and possesses good low-temperature properties. Table 7 indicates that TPU markedly improves the impact strength of POM50 from 15.21 J/m to 42.55 J/m by adding 5 wt% TPU. The impact strength continuously increases with TPU content. EGMA is a non-biodegradable

elastomer and greatly increases the impact strength of POM50 as the addition of 20 wt% EGMA improves the impact strength from 15.21 J/m to 72.25 J/m. Figure 3.8 conducted a comparison on impact strength between TPU and EGMA. TPU is more effective than EGMA on toughening POM50 since the impact strength was improved 180% by the addition of 5 wt% TPU and 74% by the same content of EGMA. The good dispersion of TPU in both PLA and POM is considered to be responsible for the better toughening effect of TPU than that of EGMA (Cheng et al., 2006).

3.4 Conclusions

DMA results showed that PLA/POM blends except for POM25 exhibited higher E´than both neat PLA and POM at temperature below T_g, exhibiting that the addition of POM increased the stiffness of PLA. HDT of PLA was improved by incorporating high content of POM (25 wt% or more). HDT of neat PLA was increased nearly 2-fold from 65.5 ^{o}C to 133 ^{o}C by adding 50 wt% POM. Heat treatment was also found to affect HDT of PLA because the HDT of POM5 was increased from 61 ^{o}C to 129.7 ^{o}C after annealing for 45 min at 85 ^{o}C. Multiple-crack structure/macroscopic phenomenon of spherulites were observed on the surface of the PLA blends containing high POM content from SEM images. Fox equation was used to identify the miscibility of the PLA/POM blends and found an estimate of 2.3 wt% POM dissolved in PLA in the case of POM50 blends, exhibiting PLA/POM blends were partially miscible. FTIR results were consistent with the Fox equation since a distinct characteristic peak observed for PLA/POM blends at 992 cm^{-1}.The toughening effect

of two type of elastomers i.e. TPU and EGMA based on the PLA/POM blend (50/50) was investigated through tensile testing. The experimental results suggested that TPU was more effectively on toughening the PLA/POM blend than EGMA.

Reference

Baiardo, M.; Frisoni, G., “Thermal and mechanical properties of plasticized poly(L-lactic acid).” Journal of Applied Polymer Science, (2003) 90 (7): 1731-1738.

Tsuji, H.; Ikada, Y., “Properties and morphologies of poly(L-lactide): 1. Annealing condition effects on properties and morphologies of poly(L-lactide).” Polymer, (1995) 36 (14): 2709-2716.

Jiang, L.; Zhang, J., “Comparison of polylactide/nano-sized calcium carbonate and polylactide/montmorillonite composites: Reinforcing effects and toughening mechanisms.” Polymer, (2007) 48: 7632-7644.

Liu, H.; Zhang, J., “Interaction of Microstructure and Interfacial Adhesion on Impact Performance of Polylactide (PLA) Ternary Blends.”Macromolecules, (2011) 44: 1513-1522.

Brizzolara, D.; Cantow, H., “Mechanism of the Stereocomplex Formation between Enantiomeric Poly(lactide)s.” Macromolecules, (1996) 29: 191-197.

Angela, M.; Harris, E., “Improving mechanical performance of injection molded PLA by controlling crystallinity.” Journal of Applied Polymer Science, (2008) 107 (4): 2246-2255.

Nanda, M.; Misra, M., “The Effects of Process Engineering on the Performance of PLA and PHBV Blends.” Macromolecular Materials and Engineering, 2011 (296) 8: 719-728.

Broz, M.; VanderHart, D., “Structure and mechanical properties of poly(D,L-lactic acid)/poly(ε-caprolactone) blends.” Biomaterials, (2003) 24 (23): 4181-4190.

Semba, T.; Kitagawa, K., “The effect of crosslinking on the mechanical properties of polylactic acid/ polycaprolactone blends.” Journal of Applied Polymer Science, (2006) 101 (3): 1816-1825.

Zhang, N.; Wang, Q., “Preparation and properties of biodegradable poly(lactic acid)/poly(butylene adipate- co -terephthalate) blend with glycidyl methacrylate as reactive processing agent.” Journal of Materials Science, (2009) 44 (1): 250-256.

Paul, DR.; Bucknall, CB., Polymer blends. New York: Wiley; 2000.

Fox, T.G., Bull. Am. Phys. Soc., (1956) 1 (123).

Sarasua, J.R.; Pouyet, J., “Dynamic Mechanical Behavior and Interphase Adhesion of thermoplastic (PEEK, PES) Short Fiber Composites.” Journal of Thermoplastic Composite Materials, (1998) 11 (1): 2-21.

Chapter 4 Conclusions

In this research, PLA/POM blends were successfully prepared through melt extrusion in this research. PLA and its blends with POM and talc were investigated by DSC, POM and XRD in detail for a comparative study of the effects of different fillers on the crystallization behavior and kinetics, and crystalline morphology. Greater enthalpy and lower cold crystallization temperature of PLA/POM blends from the DSC first heating scan exhibited improvement in crystallization ability of PLA by adding POM. Furthermore, two cold crystallization peaks were observed for the PLA/POM blends. During isothermal crystallization, $t_{1/2}$ decreased with increasing loadings of fillers, and increased with increasing crystallization temperature for both PLA/POM and PLA/talc blends. Moreover, $t_{1/2}$ of talc was much smaller than that of PLA and PLA/POM blends, exhibiting talc is more effective on improving the crystallization rate of PLA. CRC of POM5 from nonisothermal crystallization was 62.76 h^{-1}, which was greater than neat POM of 6.79 h^{-1}, suggesting significant enhancement in the crystallization rate. Polarized optical micrographs were taken to observe the crystalline morphology of PLA blends, well-defined banded spherulites were obtained only for PLA/POM blends. Transparency of PLA/POM blends was better than both PLA and PLA/talc blends, indicating PLA/POM blends were partially miscible, which was in agreement with FTIR results. XRD results displayed crystal structure of PLA was changed by the presence of POM due to the characteristic

diffraction peak of POM2 and POM5 at 22.8^{o}. Mechanical properties of neat PLA were not dramatically changed by the presence of POM and talc, which was probably due to their low loading levels.

Thermodynamic properties and phase morphology of PLA/POM blends were examined using DMA and SEM. DMA results indicated that PLA/POM blends except for POM25 exhibited higher E' than both neat PLA and POM at temperature below T_g, indicating the addition of POM increased the stiffness of PLA. Introducing T_gs derived from tan δ curve into the Fox equation, an estimate of about 2.3 wt% of POM dissolved in PLA phase of POM50 was obtained. Therefore, PLA/POM blends were considered to be partially miscible. FTIR was used to identify the miscibility of PLA/POM blends as well; the result was consistent with that of the Fox equation. HDT of PLA was increased by incorporating high content of POM (25 wt% or more). HDT of neat PLA was increased nearly 2-fold from 65.5 ^{o}C to 133 ^{o}C by adding 50 wt% POM. The improvement in HDT was attributed to the increased crystallinity of PLA by adding POM. Heat treatment was also found to affect HDT of PLA because the HDT of POM5 was increased from 61 ^{o}C to 129.7 ^{o}C after annealing for 45 min at 85 ^{o}C. From SEM images, multiple-crack structure was observed on the surface of the PLA blends containing high POM content. Mechanical properties were examined to further understand the performance of PLA/POM blends. The PLA/POM blends exhibited higher modulus than neat PLA and POM, while tensile strength and impact strength were not greatly increased by adding POM. The toughening effects of two

types of elastomers i.e. TPU and EGMA based on the PLA/POM blend (50/50) were investigated, and the experimental results suggested that TPU had better effects on toughening the PLA/POM blend than EGMA.